To the Graduate Council:

I am submitting herewith a thesis written by David Lewis Bailey entitled "Surface-enhanced Raman Scattering from Silver Ellipsoidal Particles." I have examined the final copy of this thesis for form and content and recommend that it be accepted in partial fulfillment of the requirements for the degree of Master of Science, with a major in Physics.

T. A. Callcott, Major Professor

We have read this thesis
and recommend its acceptance:

Accepted for the Council:

Vice Provost
and Dean of the Graduate School

STATEMENT OF PERMISSION TO USE

In presenting this thesis in partial fulfillment of the requirements for a Master's degree at the University of Tennessee, Knoxville, I agree that the Library shall make it available to borrowers under the rules of the Library. Brief quotations from this thesis are allowed without special permission, provided that accurate acknowledgment of the source is made.

Permission for extensive quotation from or reproduction of this thesis may be granted by my major professor, or in his absence, by the Head of Interlibrary Services when, in the opinion of either, the proposed use of the material in this thesis is for scholarly purposes. Any copying or use of the material in this thesis for financial gain shall not be allowed without my written permission.

Signature Dawn Lewis Bailey

Date July 26, 1988

SURFACE-ENHANCED RAMAN SCATTERING FROM SILVER ELLIPSOIDAL PARTICLES

A Thesis

Presented for the

Master of Science

Degree

The University of Tennessee, Knoxville

David Lewis Bailey

August 1988

DEDICATION

I would like to dedicate this thesis to my parents Clay and Carol Bailey. Without their love and support, I would not have survived graduate school.

ACKNOWLEDGEMENTS

I would like to express my gratitude to my major professor, Dr. Tom A. Callcott, who guided me through the research that culminated in this thesis. His knowledge and expertise made the road upon which I have travelled a smoother one. I would also like to express my gratitude to Dr. Tom L. Ferrell and Dr. R. J. Warmack for providing theoretical and experimental guidance throughout the course of this project. A special thanks goes to Milan Buncick for "showing me the ropes" around the lab and being there when I needed help. My thanks also goes out to Brenda Thomas for her valuable assistance in the preparation of this document.

I would also like to thank my family and friends for their love and support during the course of my work in college. They made the journey a more pleasant one.

ABSTRACT

The wavelength dependence of surface-enhanced Raman scattering from molecules adsorbed on the dry surfaces of silver ellipsoids has been measured. Several substrates were employed during the measurements: silver coated, random arrays of silicon dioxide posts, silver coated polystyrene spheres, and silver metal island films. The Raman active compounds used were phthalic acid and benzoic acid. The data for the silicon dioxide posts are representative of the data for all of the substrates; therefore, only the post data is presented.

Since these substrates consist of submicron sized particles of silver which are known to have surface plasmon resonances for optical energies, it was logical to assume that SERS could be explained in terms of the field enhancement due to the surface plasmons. The data, however, indicates that there is a significant chemical dependence in the SERS that cannot be correlated with the generation of surface plasmon resonances of the surface particles. The SERS peak positions and widths do not correspond to those of the surface plasmon resonances of the surface particles; therefore, there is not good agreement with the theory.

SERS data was obtained with several laser wavelengths throughout the visible portion of the spectrum. The optical properties of the surface particles were obtained by measuring the optical absorbance of the substrates.

TABLE OF CONTENTS

LIST OF FIGURES

FIGURE PAGE

INTRODUCTION

The discovery of Raman scattering by C. V. Raman in 1928 gave scientists a new and exciting tool for unlocking the secrets of the molecular world. By measuring the color shift of light tramsmitted through solutions, Raman was able to spectroscopically identify the chemical compounds in the solutions. Many theoretical and experimental advances have been made since this discovery. The most noticeable of these advances was the advent of the laser. Raman spectroscopy is now a well developed field which provides vast information about the molecular world. The field was expanded in 1977 when surface-enhanced Raman scattering (SERS) was discovered. Since then, much research has been performed to illuminate the details of molecular spectra on surfaces. The body of SERS related literature presently includes over fifteen-hundred papers.

SERS was first detected in 1974 by Fleishmann, et al., while measuring the Raman spectrum of aqueous pyridine adsorbed on roughened silver electrodes (I.1). He noticed that the Raman scattering intensity increased tremendously after several oxidation-reduction cycles of the silver electrodes. Fleischmann postulated that the signal enhancement was due to a significant increase in the number of adsorbed molecules. His hypothesis has since been found to be inadequate. Fleischmann's experiments were repeated by Jeanmaire and Van Duyne in 1977 (I.2). Quantitative coulombic measurements were performed on silver electrodes

roughened by one oxidation-reduction cycle. The scattering cross section of pyridine was measured to have increased by a factor of 10^5 to 10^6 over the normal scattering cross section. This factor cannot be obtained by using Fleischmann's original model as was pointed out by Van Duyne. Furthermore, it was found that silver works significantly better as a substrate than any other material.

Theories have been proposed to explain the enhancement in terms of electromagnetic effects and chemical interactions between the adsorbed molecules and the metal substrates. Electromagnetic theories focus on the field interactions between the incident field, the metal particles, and the Raman active molecule. Chemical interaction theories focus on the effects that substrates have on the energy level structure of the adsorbed molecule.

SERS has been measured on several forms of metal particles in addition to silver electrodes. Creighton, et al., measured the wavelength dependence of the enhancement in gold and silver sol solutions (I.3). Liao, et al., formed silver particles on ordered arrays of silicon dioxide posts (I.4). Less impressive measurements of the enhancement have been made on other surfaces including reflection gratings coated with silver.

The contents of this thesis are an analysis of the Raman scattering enhancement properties of silver coated, random arrays of silicon dioxide posts etched into the surface of quartz microscope slides. Several other types of substrates were tested during this lengthy experiment: silver coated polystyrene spheres, silver metal island

films, and slanted silicon dioxide posts. The post data results are representative of the body of SERS data; therefore, only the post data will be discussed. Two Raman active compounds--benzoic acid and phthalic acid--were used for comparison. Optical absorbance data on each substrate was also taken. A one dimensional classical model of light scattering from a free molecule is presented as a guide to data interpretation.

CHAPTER I

THEORY

Introduction

This chapter contains a brief discussion of Raman scattering, SERS theory, and a one dimensional, classical derivation of the Raman scattering cross-section for a free molecule. There is also a discussion of a model for the optical properties of spheroids, and two graphs of the surface plasmon resonances of a model prolate silver particle. This model does not include substrate effects.

When light impinges on a molecule, it may be scattered elastically or inelastically. If the scattered light has the same frequency as the incident light, then there is no net energy gain or loss to the molecule. This is called Rayleigh scattering. If the scattered light does not have the same frequency as the incident light, then there is a net energy transfer between the molecule and the light. This is called Raman scattering (1.1).

Light scattering arises from dipole moments induced in the molecule by the incident field. The induced dipole moment is proportional to the incident electric field and the polarizability of the molecule. If the polarizability of a vibrational or rotational mode of the molecule is not a function of the nuclear separation, then there will not be Raman scattering. There may, however, be Rayleigh scattering (1.2).

At room temperature, most molecules will be in the ground state. Raman scattering in this case will produce a negative frequency shift in the scattered light. Some molecules, however, may be in an excited state. If a molecule makes a transition to a lower energy level during the scattering process, then the scattered light will retain the excess energy and undergo a positive frequency shift. The spectral lines produced with a frequency drop are called Stokes lines, and the lines due to a frequency increase are called anti-Stokes lines. Anti-Stokes lines are about a factor of 100 less in intensity than Stokes lines (1.3).

Models of SERS usually adhere to one of two approaches: electromagnetic or chemical. The first approach assumes that the enhancement is due strictly to electromagnetic interactions between the molecule, the surface, and the incident field. One commonly modeled electromagnetic phenomenon is the surface plasmon. The fields generated by the incident light and a surface plasmon can be quite intense. These fields are the polarizing forces acting on the molecules residing on the surface. One major feature of this theory is the close relationship between the generation of surface plasmons and the wavelength dependence of the enhancement. Since the intensity of the plasmon field is a function of the surface curvature, particles with sharp surface features can generate field enhancements greater than those possible on smooth surfaces. This is called the "lightning rod" effect (1.4).

In another model, the enhancement is explained as a dipole field induced resonance between the molecule and the incident laser field. The polarizing field of the plasmon alters the molecule's energy level

structure so that resonant Ramam or pre-resonant Raman scattering may occur (1.5). Electromagnetic theories also tend to not be molecule specific.

Chemical interactions may also play an important role in SERS. Changes in the polarizability of the molecule due to charge transfer may be a function of the substrate material and morphology. This may account for the Raman enhancement (1.6). Adsorption or chemisorption of the molecule with the surface may drastically alter the polarizability of certain rotational or vibrational modes thereby allowing the molecule to be easily polarized by the incident light.

The selection rules for transitions involved in Raman scattering may be altered by the electromagnetic effects and the chemical effects.

Calculations

The model presented here for light scattering from a molecule includes Rayleigh scattering as well as Raman scattering. It is based on the Heisenberg-Kramers dispersion relation (1.7). The transitions of excited electrons are viewed classically as harmonic oscillators of resonant frequency ω_e.

Newton's equation of motion for the displacement from equilibrium of an electron in a molecule can be written as

$$\frac{dx^2}{dt^2} + \Gamma\frac{dx}{dt} + \omega_e{}^2 x = \frac{-e}{m} E(t), \qquad [1.1]$$

where Γ is a damping factor, $-e$ the electron charge, and m the electron

mass. This is a one-dimensional model with x in the direction of polarization of the incident light. Also, E(t) is the incident light's time-varying electric field. The wavelength of the light is assumed to be much larger than the target molecules. If the electric field is assumed to be of magnitude

$$E(t) = E_o e^{-i\omega_o t}, \qquad [1.2]$$

then the steady-state solution to [1.1] is

$$x = \frac{(-eE_o/m)e^{-i\omega_o t}}{-\omega_o^2 - i\,\Gamma\omega_o + \omega_e^2}. \qquad [1.3]$$

For the most general case, the nuclei of the molecule are assumed to oscillate about their equilibrium positions. The shapes of the electron clouds are altered by the stretching of the nuclear motions; therefore, the electronic resonances are functions of the nuclear displacements. If the nuclear motion is restricted to small displacements from equilibrium, then the appropriate differential equation for the displacement of the nuclei is

$$\frac{d^2y}{dt^2} + \omega_m^2 y = 0, \qquad [1.4]$$

where ω_m is the natural angular frequency of the vibration, and where

$$y = \frac{y_o}{2} e^{-i\omega_m t} + \frac{y_o}{2} e^{i\omega_m t}. \qquad [1.5]$$

The phase is chosen for convenience so that $y=y_o$ at time $t=0$.

The electronic resonances vary with y, and y_o is usually a small fraction of an Angstrom. Therefore, $\omega_e^2(y)$ may be expanded in a Taylor series about y=0 to yield

$$\omega_e^2(y) = \omega_e^2(0) + 2\,\omega_e(0)\left[\frac{d\omega_e(y)}{dy} \Big|_{y=0} \right] y, \qquad [1.6]$$

For convenience, let

$$\beta = 2\omega_e(0)\left[\frac{d\omega_e(y)}{dy} \Big|_{y=0} \right]. \qquad [1.7]$$

The correction to the electronic displacement x due to the nuclear motion is small. The new diplacement may be written as $x = \bar{x} + \delta x$ where $\bar{x}$ is the previously treated displacement in [1.1]. Terms of order $(\delta x)^2$ and $y\delta x$ are neglected in the expansion of x. Inserting $x = \bar{x} + \delta x$ into the equation of motion for the electronic displacement allows inspection of the individual terms to determine which may be neglected. Thus, one uses

$$\frac{d^2x}{dt^2} + \Gamma\frac{dx}{dt} + \omega_e^2(y)x = \frac{-e}{m} E(t), \qquad [1.8]$$

Let the operator D be defined by

$$D = \frac{d^2}{dt^2} + \Gamma\frac{d}{dt} + \omega_e^2 \quad . \qquad [1.9]$$

Employing [1.7], [1.9], and $x = \bar{x} + \delta x$ transforms [1.8] into

$$D(\bar{x} + \partial x) = \frac{-e}{m} E(t). \qquad [1.10]$$

Eq. [1.10] contains the orginal equation of motion [1.1] for the case of oscillation about the equilbrium position written in terms of the new varible $\bar{x}$.

$$\frac{d^2\bar{x}}{dt^2} + \Gamma\frac{d\bar{x}}{dt} + \omega_e^2\bar{x} = \frac{-e}{m} E(t). \qquad [1.11]$$

Using [1.11] in [1.10], the differential equation for the displacement δx may now be written as

$$\frac{d^2\delta x}{dt^2} + \Gamma\frac{d\delta x}{dt} + \omega_e^2\delta x + \beta y\bar{x} = 0, \qquad [1.12]$$

where the term $\beta y\delta x$ has been neglected. Eq.'s [1.3] and [1.5] may be used to write the product $\beta y\bar{x}$ as

$$\beta y\bar{x} = \frac{(-eE_o y_o \beta/2m)e^{-i(\omega_o-\omega_m)t}}{(\omega_e^2 - \omega_o^2 - i\Gamma\omega_o)}. \qquad [1.13]$$

Terms involving $\omega_o+\omega_m$ are not retained as they eventually may be seen to coincide with energy gain which is a process of low probability at room temperature. Eq. [1.12] may now be written as

$$\frac{d^2\delta x}{dt^2} + \Gamma\frac{d\delta x}{dt} + \omega_e{}^2\delta x = \frac{(eE_o y_o \beta/2m)e^{-i\omega_1 t}}{(\omega_e{}^2 - \omega_o{}^2 - i\Gamma\omega_o)}, \qquad [1.14]$$

where $\omega_1 = \omega_o-\omega_m$.

The steady state solution to [1.13] is

$$\delta x = \frac{(eE_o y_o \beta/2m)e^{-i\omega_1 t}}{(\omega_e{}^2 - \omega_o{}^2 - i\Gamma\omega_o)(\omega_e{}^2 - \omega_1{}^2 - i\Gamma\omega_1)}. \qquad [1.15]$$

Therefore, the total displacement $x = \bar{x} + \delta x$ may be obtained from [1.3] and [1.15]

$$x = \frac{(eE_o/m)e^{-i\omega_o t}}{(\omega_e{}^2 - \omega_o{}^2 - i\Gamma\omega_o)} +$$

$$\frac{(eE_o y_o \beta/2m)e^{-i\omega_1 t}}{(\omega_e{}^2 - \omega_o{}^2 - i\Gamma\omega_o)\ (\omega_e{}^2 - \omega_1{}^2 - i\Gamma\omega_1)}, \qquad [1.16]$$

The final form for the equation of motion of the electron may be written with two driving forces in the inhomogenous part. The first term represents the driving force on the electron produced by the incident

light. The second term represents a correction to the driving force produced by the motion of the oscillating nuclei.

$$\frac{d^2x}{dt^2} + \Gamma\frac{dx}{dt} + \omega_e^{\,2} = \frac{-e}{m} E_o e^{-i\omega_o t} + \frac{(eE_o y_o \beta/2m)e^{-i\omega_1 t}}{(\omega_e^{\,2} - \omega_1^{\,2} - i\Gamma\omega_1)} \qquad [1.16]$$

$$= \frac{F_o}{m} e^{-i\omega_o t} + \frac{F_1}{m} e^{-i\omega_1 t} \qquad [1.17]$$

$$= \frac{F_o(t)}{m} + \frac{F_1(t)}{m}. \qquad [1.18]$$

The next step in this analysis is the calculation of the power expenditure of the molecule during an arbitrary length of time. Manipulation of [1.1] reveals that the rate of energy dissipation by the molecule is equal to the time average of $\dot{x}F$ where F is the net force acting on the electron. This result may be obtained by first writing the left side of [1.1] as the first derivative of the total energy of the electron for the case of no damping (i.e. Γ=0). The average of dW/dt over an arbitrary number of cycles is simply the average of the right side, $\dot{x}F$, over the same number of cycles. Calculation of this quantity involves the integration of many terms. A more concise and less time consuming method of calculation the power dissipation is obtained by using [1.19]. Eq. [1.19] was obtained by combining the force terms in [1.18] and the electronic displacements $\bar{x}$ and δx.

$$\langle \dot{x}F \rangle = {}^1/_2 \, \mathrm{Re}[\, \dot{\bar{x}} \, F_o^{\,*}(t)] + {}^1/_2 \, \mathrm{Re}[\, \delta\dot{x} \, F_1^{\,*}(t)]. \qquad [1.19]$$

Eq. [1.19] will be referred to later.

It is necessary to calculate the polarizability of the molecule so that the scattering cross section may be determined. First, the induced dipole moment must be found. The definition of the induced dipole moment is p = qx where q is the charge, and x is the previously analyzed net electronic displacement. Therefore,

$$p = -ex = \frac{(e^2\ E/m)e^{-i\omega_o t}}{(\omega_e^{\ 2} - \omega_o^{\ 2} - i\Gamma\omega_o)} -$$

$$\frac{(e^2 E_o y_o \beta/2m)e^{-i\omega_1 t}}{(\omega_e^{\ 2} - \omega_o^{\ 2} - i\Gamma\omega_o)(\omega_e^{\ 2} - \omega_1^{\ 2} - i\Gamma\omega_1)}, \qquad [1.20]$$

Or
$$p = \alpha_o E_o e^{-i\omega_o t} - \alpha_1 E_o e^{-i\omega_1 t}. \qquad [1.21]$$

In order to simplify the calculations, consider the following approximation. Let

$$\frac{y_o\beta}{\omega_e^{\ 2} - (\omega_o - \omega_m)^2 - i\Gamma(\omega_o - \omega_m)} =$$

$$\frac{y_o\beta}{(\omega_e^{\ 2} - \omega_o^{\ 2} - i\Gamma\omega_o)\left[1 + \dfrac{2\omega_o\omega_m + i\Gamma\omega_m - \omega_m^{\ 2}}{(\omega_e^{\ 2} - \omega_o^{\ 2} - i\Gamma\omega_o)}\right]} \qquad [1.22]$$

$$\approx \frac{y_o\beta}{(\omega_e^{\ 2} - \omega_o^{\ 2} - i\Gamma\omega_o)}. \qquad [1.23]$$

The dipole moment may then be approximated as

$$p = \frac{(eE_o/m)e^{-i\omega_o t}}{(\omega_e^2 - \omega_o^2 - i\Gamma\omega_o)} - \frac{(eE_o\beta/2m)e^{-i\omega_1 t}}{(\omega_e^2 - \omega_o^2 - i\Gamma\omega_o)}. \qquad [1.24]$$

Inspection of [1.24] reveals the following connection between α_o and α_1.

$$\alpha_o = \frac{e^2/m}{(\omega_e^2 - \omega_o^2 - i\Gamma\omega_o)}, \qquad [1.25]$$

$$\frac{\partial\alpha_o}{\partial y} = \frac{(-e^2/m)(\partial\omega_e^2/\partial y)}{(\omega_e^2 - \omega_o^2 - i\Gamma\omega_o)^2}, \qquad [1.26]$$

$$\left.\frac{\partial\alpha_o}{\partial y}\right|_{y=0} = \frac{-e\beta/m}{(\omega_e^2 - \omega_o^2 - i\Gamma\omega_o)^2}. \qquad [1.27]$$

This form of the polarizability may be used to write the dipole moment as

$$p = \alpha E_o e^{-i\omega_o t} + \left[\left.\frac{\partial\alpha_o}{\alpha y}\right|_{y=0}\right]\frac{1}{2} y_o E_o e^{-i\omega_1 t}. \qquad [1.28]$$

The dipole moment written in vector form is

$$\mathbf{p} = \alpha E_o e^{-i\omega_o t} + \left.\frac{\partial\alpha}{\partial y}\right|_{y=0} \frac{y_o}{2} E_o e^{-i\omega_1 t}. \qquad [1.29]$$

Scattering from a dipole with moment **p** in the far field approximation is described by [1.29] from reference (1.8).

$$E_{sca} = \frac{\omega^2 e^{ik\cdot r}}{c^2 r}[(n \times p) \times n], \qquad [1.30]$$

where the unit vector **n** is in the direction of observation, and r is the distance from the dipole center. Inserting **p** into [1.30] gives

$$E_{sca} = \frac{\omega_o^2 e^{ik\cdot r}}{c^2 r}[(n \times E_o) \times n]\left[\alpha_o e^{-i\omega_o t} + \gamma_o e^{-i\omega_1 t}\right], \qquad [1.31]$$

where

$$\alpha_o = \alpha, \qquad [1.32a] \qquad \gamma_o = \frac{\partial \alpha_o}{\alpha y}\Big|_{y=0} \frac{y_o}{2}, \qquad [1.32b]$$

Manipulation of [1.30] gives

$$E_{sca} = \frac{\omega_o^2 e^{ik\cdot r}}{c^2 r}[E_o - n(n\cdot E)]\left[\alpha_o e^{-i\omega_o t} + \gamma_o e^{-i\omega_1 t}\right]. \qquad [1.33]$$

It is also necessary to know the magnetic component of the scattered wave.

$$H_{sca} = n \times E_{sca}\ , \qquad [1.34]$$

where

$$H_{sca} = \frac{\omega_o^2 e^{ik\cdot r}}{c^2 r}[n \times E_o]\left[\alpha_o e^{-i\omega_o t} + \gamma_o e^{-i\omega_1 t}\right]. \qquad [1.35]$$

Separating E_{sca} and H_{sca} into their respective ω_o and ω_1 dependent components permits the use of [1.36] to calculate the Poynting vector **S** for the scattered wave (1.9).

$$\mathbf{S} = \frac{c}{8\pi} \mathbf{E} \times \mathbf{H}^{*} \qquad [1.36]$$

The Poynting vector represents the time average flux of energy per unit area per unit time. Separating the scattered wave components into their ω_0 and ω_1 dependent parts gives

$$E^{o}_{sca} = \frac{\omega_o^2 e^{ik\cdot r}}{c^2 r} [(n \times E_o) \times n] \alpha_o e^{-i\omega_o t}, \qquad [1.37]$$

$$E^{1}_{sca} = \frac{\omega_o^2 e^{ik\cdot r}}{c^2 r} [(n \times E_o) \times n] \gamma_o e^{-i\omega_1 t}, \qquad [1.38]$$

$$H^{o}_{sca} = \frac{\omega_o^2 e^{ik\cdot r}}{c^2 r} [n \times E_o] \alpha_o e^{-i\omega_o t}, \qquad [1.39]$$

$$H^{1}_{sca} = \frac{\omega_o^2 e^{ik\cdot r}}{c^2 r} [n \times E_o] \gamma_o e^{-i\omega_1 t}. \qquad [1.40]$$

Eq. [1.19] reveals that the real part of the complex form of the time average of the energy dissipation must be taken in order to obtain the correct answer. Therefore, inserting terms with comparable exponents into [1.36] and taking the real part gives

$$\langle \mathbf{S} \rangle = \frac{c}{8\pi} \left[\mathrm{Re}(E^{o}_{sca} \times H^{o}_{sca}) + \mathrm{Re}(E^{1}_{sca} \times H^{1}_{sca}) \right]. \qquad [1.41]$$

In order to solve [1.40], the cross product appearing in both terms must be simplified.

$$E_{sca} = \frac{\omega_o^2 e^{ik\cdot r}}{c^2 r} [(n \times p) \times n], \qquad [1.42]$$

$$E_{sca} = \frac{\omega_o^2 e^{ik\cdot r}}{c^2 r} [p - n(p\cdot n)]. \qquad [1.43]$$

Eq [1.43] may also be used to simplify [1.40].

$$H_{sca} = n \times E_{sca} = \frac{\omega_o^2 e^{ik\cdot r}}{c^2 r} [n \times p]. \qquad [1.44]$$

Therefore,

$$E_{sca} \times H_{sca}^{*} = \frac{\omega_o^4}{c^4 r^2} \left[[p - n(n\cdot p)] \times [n \times p^{*}]\right] \qquad [1.45]$$

$$= \frac{\omega_o^4}{c^4 r^2} \left[n(p\cdot p^{*}) - n(n\cdot p)(n\cdot p^{*})\right]. \qquad [1.46]$$

Eq [1.46] may now be written

$$E_{sca} \times H_{sca}^{*} = |\alpha|^2 \frac{\omega_o^4}{c^4 r^2} \left[|E_o|^2 - (n\cdot E_o)(n\cdot E_o^{*})\right] n. \qquad [1.47]$$

From the definition of the differential scattering cross section (1.10),

$$\frac{d\sigma}{d\Omega} = \frac{8\pi r^2 \langle S \rangle}{c|E_o|^2}, \qquad [1.48]$$

the following equation may be written for Rayleigh and Raman scattering.

$$\left(\frac{d\sigma}{d\Omega}\right)_{total} = \frac{\omega_o^4}{c^4}\frac{|\alpha_o|^2}{|E_o|^2}\left[|E_o|^2 - (\mathbf{n}\cdot\mathbf{E}_o)(\mathbf{n}\cdot\mathbf{E}_o^*)\right] +$$

$$\frac{\omega_o^4}{c^4}\frac{|\gamma_o|^2}{|E_o|^2}\left[|E_o|^2 - (\mathbf{n}\cdot\mathbf{E}_o)(\mathbf{n}\cdot\mathbf{E}_o^*)\right]. \qquad [1.49]$$

The first term represents the Rayleigh scattering, and the second term represents the Raman scattering. Finally, [1.20] through [1.24] demonstrate that γ_o is an approximation of the polarizability evaluated at the Raman shifted frequency ω_1. If the Raman shifted polarizability is evaluated directly from the second term in [1.20], then γ_o is written

$$\gamma_o = \alpha(\omega_o)\alpha(\omega_1)\frac{1}{2}y_o\beta\frac{m}{e^2}. \qquad [1.50]$$

The Raman scattering cross section may be written as

$$\left(\frac{d\sigma}{d\Omega}\right)_{Raman} = \frac{\omega_o^4}{c^4}|\alpha(\omega_o)\alpha(\omega_1)|^2\frac{y_o^2\beta^2m^2}{4e^2}\left[1 - \frac{(\mathbf{n}\cdot\mathbf{E}_o)(\mathbf{n}\cdot\mathbf{E}_o^*)}{|E_o|^2}\right] \qquad [1.51]$$

$$= \frac{\omega_o^4}{c^4}|\alpha(\omega_o)\alpha(\omega_1)|^2\frac{y_o^2\beta^2m^2}{4e^4}[1 - \cos^2\Theta], \qquad [1.52]$$

where Θ is the angle between the electric field vector E of the incident light and the observation normal **n**.

There are several factors influencing the differential cross-section that warrant a closer look. The ω_o^4 dependence indicates that the probability of scattering will increase with the frequency of

the excitation light. This dependence is removed during the data analysis. Eq.'s [1.6] and [1.7] indicate that the β^2 dependence of the scattering cross-section will be greatest for molecules with electronic frequencies that vary significantly with nuclear diplacement from equilibrium.

The molecular polarizability is written as the product of the polarizability evaluated at the incident frequency and the Raman shifted frequency, therefore, both factors must be included. According to this model, it is possible to measure two maxima in the scattering cross-section if the frequency separation is sufficiently large.

The angular dependence of the scattering cross-section expressed in the $[1 - \cos^2\theta]$ term indicates that scattering will be greatest in the direction colinear with **n**.

The model illustrated in the preceding text applies to bulk Raman scattering for free molecules. A model for SERS from silver particles is required. Silver is known to have strong surface plasmon resonances with low damping in the visible portion of the spectrum. The resulting field enhancements can be quite large. The Raman scattering cross-section is also dependent on the intensity of the incident electric field. Therefore, the relationship between the SERS enhancement and the positions and intensities of the surface plasmon resonances were investigated. These resonances are dependent on the particle shapes and the dielectric function of the material. It is necessary to model the surface optical properties in order to relate the SERS theory to the data.

The surfaces of the SERS samples examined in this text consisted of ellipsoids of various shapes and sizes. A model that includes a combination of several particle shapes is necessary in order to describe the optical properties of the surface. This is done in the manner prescribed in (1.11). The surface can be modeled as a collection of prolate and oblate spheroids. The axis ratios of a particular shape may be obtained from the optical data for the surface. For instance, a substrate with a resonance in the red for p-polarized light may be partially modeled as prolate spheroids with low axis ratios. Likewise, a substrate with a resonance in the blue for s-polarized light may be modeled as oblate spheroids with high axis ratios. It is not necessary, however, to only associate oblate particles with s polarization resonances and prolate particles with p polarization resonances. A combination of the two with the appropriate fitting constants will describe the surface.

As an example, consider the following model for the differintial scattering cross-section of silver prolate spheroid surrounded by a thin layer of benzoic acid. The following graphs in figures 1.1 and 1.2 are plots of the surface plasmon resonances of the particle (1.12). The surface plasmon resonances are calculated by solving the electrostatic boundary value problem in prolate spheroidal coordinates. For this particle, the surface plasmon energy for oscillations along the minor axis is approximately 3.5 eV (360 nm). Likewise, the surface plasmon energy for oscillations along the major axis is 2.4 eV (520 nm). In this model, if the electric field of the incident light is coplanar with the major post axis, then the high energy oscillations will be generated by

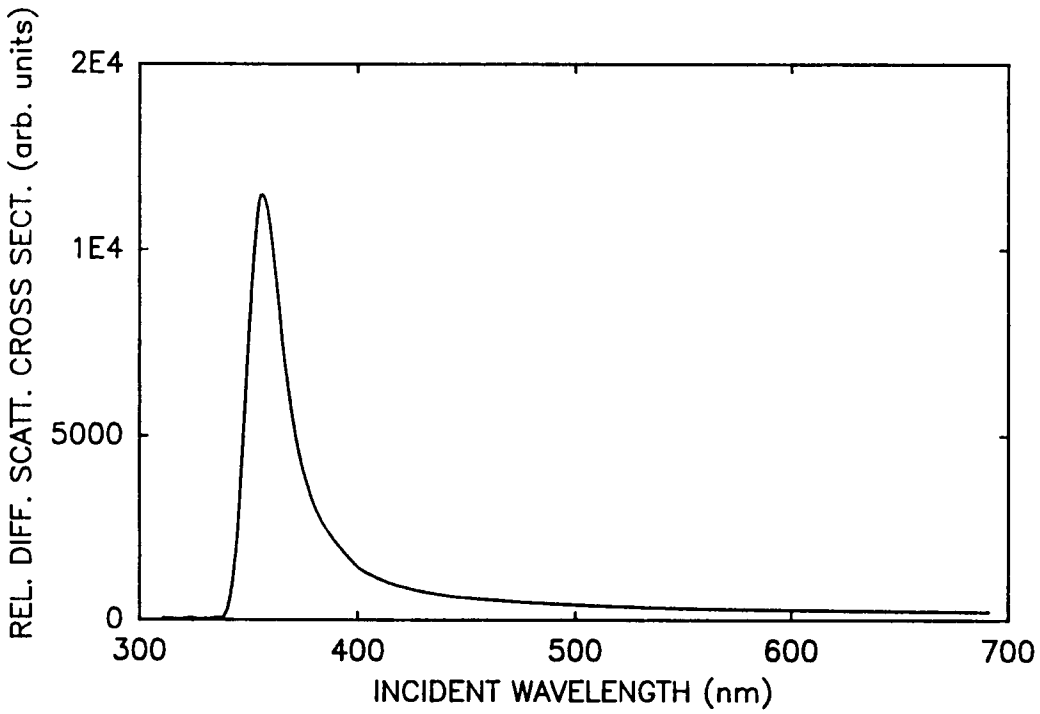

Figure 1.1. The relative differential scattering cross-section of the prolate spheroid for s-polarized light.

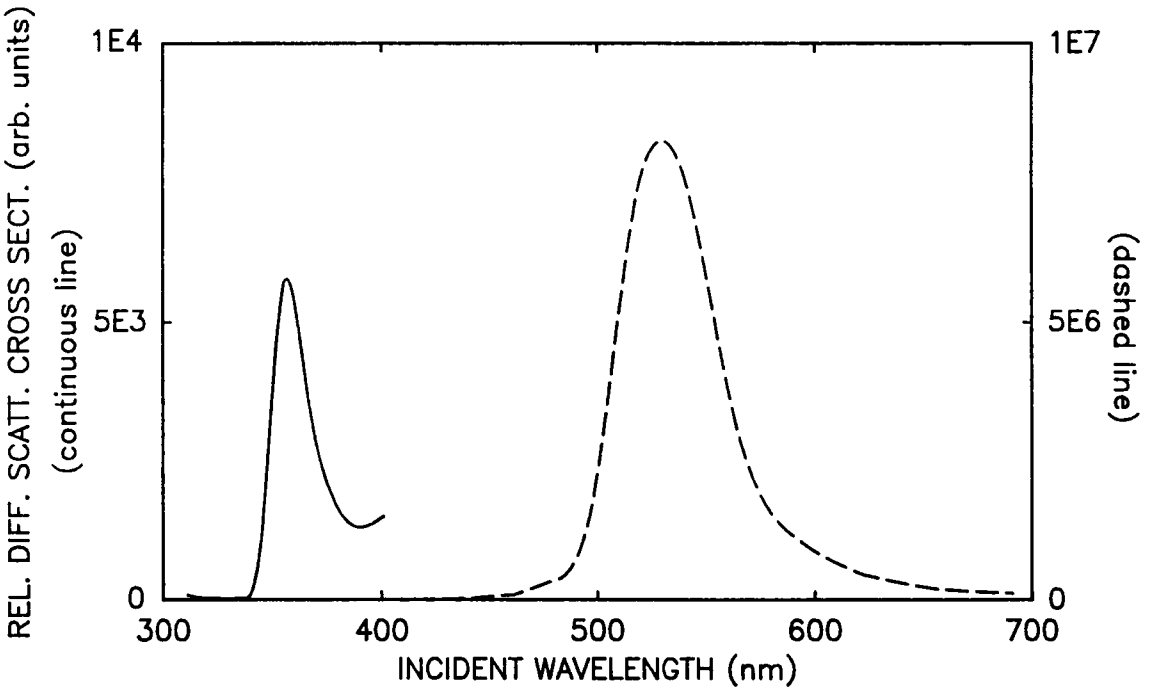

Figure 1.2. The relative differential scattering cross-section of the prolate spheroid for p-polarized light. The continuous line corresponds to the limits on the left-hand y axis, and the dashed line corresponds to the limits on the right-hand y axis. Both lines are portions of the same curve.

the s-polarized component of 360 nm wavelength light and the low energy oscillations by the p-polarized component of 520 nm wavelength light. If, however, the electric field vector is coplanar with the minor post axis, then both polarizations of the incident light at 360 nm will generate the high energy resonance.

These data are representative of the surface plasmon resonances for the substrates used in the experiments.

CHAPTER II

EXPERIMENTAL PROCEDURES

Substrate Synthesis

The samples used in the analysis of the Raman enhancement were constructed according to the method developed by J. W. Little and M. C. Buncick (2.1). These samples consist of well defined submicron posts etched from a thin layer of vacuum deposited silicon dioxide on the surfaces of fused silica slides. The process was optimized to develop samples with posts that have an aspect ratio of about 3:1. Raman active microstructures were formed by evaporating discontinuous metal films of silver on these slides at various angles of incidence.

As mentioned previously, the SERS enhancement of silver coated spheres were also tested (2.2). The sphere substrates were made by first diluting a 10 percent by weight sphere solution in distilled water. Two concentrations of spheres were tested: three percent and one percent. A few drops of the sphere solution were then spin coated onto a clean, fused silica microscope slide. The sphere coverage was regulated by adjusting the spin coating angular velocity (rpm). The angular velocities that were employed ranged from 900 rpm to 1500 rpm. Silver was then vacuum deposited on the sample at an angle to the substrate normal. The sample was rotated during the evaportion. The sphere sizes used were 176 nm, 243 nm, and 460 nm.

The metal island film substrates were made by depositing a thin film of silver onto a clean, fused silica microscope slide under vacuum at normal incidence (2.3). The evaporation thicknesses for the films tested were between 4 nm and 10 nm. The slide was then heat treated on a laboratory hot plate at 300 C for one minute in order to generate the oblate spheriod film.

Fused silica microscope slides (2.4) with dimensions 1 in. x 3 in. were broken into 1 in. x 1 in. sections using a carbide glass cutting tool. The sections were then ultrasonically cleaned in a dilute solution of laboratory detergent and distilled water (2.5). The slides were then rinsed in a continuously flowing stream of distilled water for at least ten minutes in order to remove any detergent residue. The slides were then ultrasonically cleaned in acetone for ten minutes and methanol for ten minutes.

Fused silica slides were used in order to facilitate optical absorbance measurements on the samples. However, it etches far too slowly to be useful as post material. This problem was overcome by evaporating a thin layer of silicon dioxide onto the slides. The vacuum system is a cryopumped electron beam evaporator (2.6) equipped with an adjustable sample mount and a quartz crystal thickness monitor. Clean slides were placed in the system at normal incidence to the evaporant, and the system was evacuated. A 300 nm layer of silicon dioxide from fused silica was deposited on the surfaces at a rate of about 0.3 nm per second. A base pressure of at least $5x10^{-7}$ torr was essential in order to achieve good adhesion between the slides and the evaporant.

When a thin silver film of approximately 10 nm or less is evaporated onto a microscope slide, the metal forms discrete islands of silver from which an etch mask may be made. For the sample used here, an evaporation was made to deposit a 5 nm layer of silver on the slide. The sample was then heat treated at a temperature of 300 C for one minute on a laboratory hot plate. This procedure generated an etch mask of silver oblate spheroids. The spheroid dimensions were on the order of 60 nm wide and 20 nm tall. They were separated by a distance of approximately 20 nm edge-to-edge. An electron micrograph of the etch mask may be found in figure 2.1.

The slides were then individually placed in a standard 13.5 MHz rf sputter-etcher for anisotropic etching (2.7). The system is equipped with an oil based diffusion pump and an in-line needle valve for precise pressure regulation. The rf power, dc bias, and gas pressure were continuously regulated and monitored. The anode served as the platform for the slide during the etch process. The system was flushed and roughed out with the etchant gas freon 23 (CHF_3) three times before being brought down to the base pressure of $5x10^{-5}$ torr. The freon pressure inside the chamber was adjusted to 2 microns. An rf input power of 50 watts and a dc bias of 100 volts were used during the etching process. In order to begin the etching process, the rf power was throttled from zero to 50 watts in about one second. The dc bias was then quickly adjusted. The optimum etching time was empirically determined to be 30 minutes. Etch times longer than 30 minutes yielded shorter posts. The silver particles that constitute the mask were removed by then so that further etching only decreased the post heights.

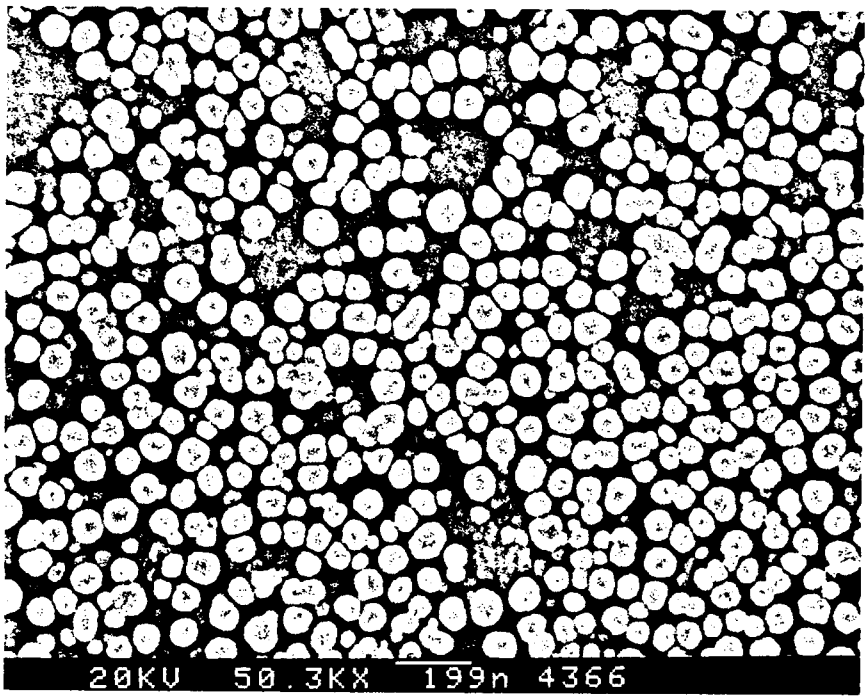

Figure 2.1. Electron micrograph of a silver oblate spheroid etch mask.

Bias potentials higher than 100 volts tended to sputter the etch mask off of the surface too quickly thereby decreasing the final post height.

This technique produced a random array of posts that are approximately 200 nm tall and 60 nm in diameter. The electron micrographs on pages 48 and 49 reveal that the major post axes are parallel to each other and the substrate normal. It is also possible to produce posts that have major axes that are tilted with respect to the substrate normal (2.8). There is a distribution of particle sizes with a typical separation distance of less than one post diameter.

The post sample was immersed in a solution of nitric acid following the etch process in order to remove any remaining portions of the etch mask. After rinsing in distilled water and ultrasonically cleaning in methanol, the slide was then placed in the cryopump evaporator. The slide was oriented so that the post axes and substrate normal were tilted at an angle to the evaporant crucible. An oblique evaporation of silver was performed in order to produce Raman active silver ellipsoids on the sides of the posts. It is possible to make particles with different aspect ratios by varying the angle of evaporation. Figure 2.2 illustrates the process. Shadowing of neighboring posts during the evaporation reduced the amount of silver being deposited on the substrate in between the posts.

The final step in the process was the doping of a Raman active compound onto the surface of the post sample. Two compounds were used in the sample analysis--benzoic acid and phthalic acid. A sample was doped with only one compound at a time. The SERS samples were usually spin coated with the Raman active compound in solution; however, the

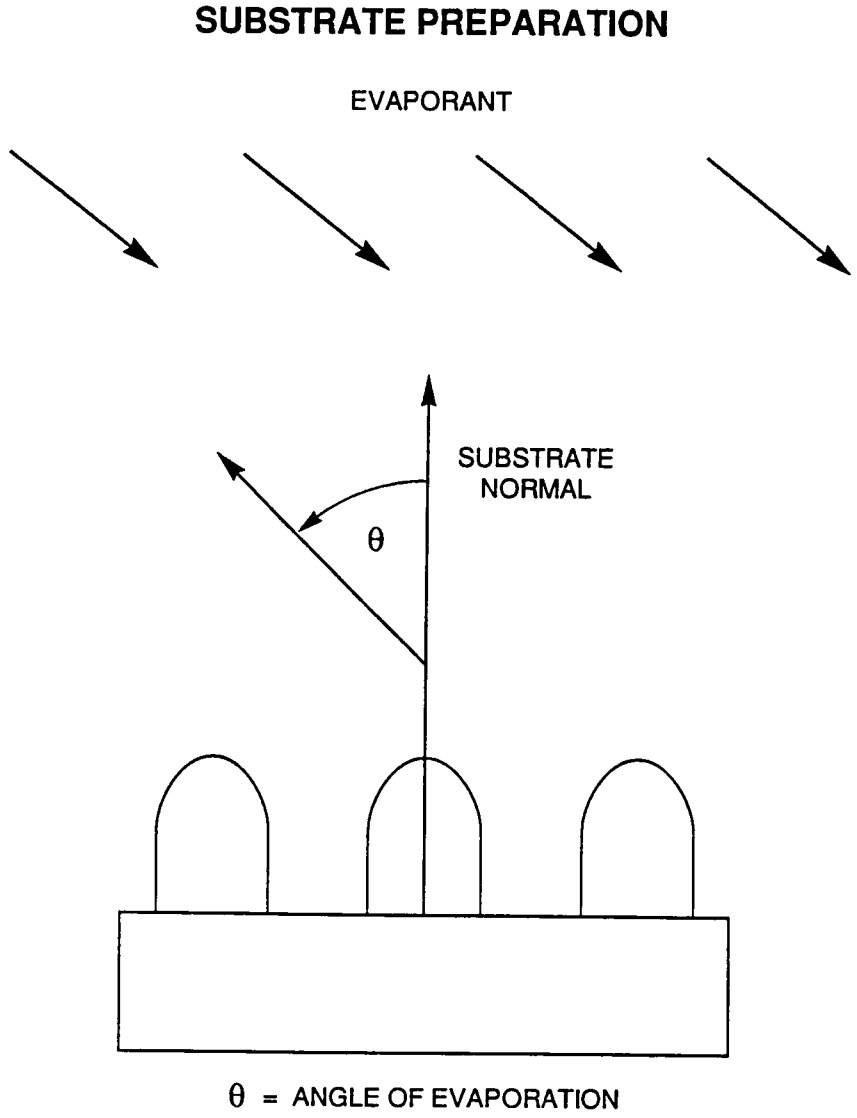

Figure 2.2. The substrate preparation process. The angle θ is the evaporation angle relative to the major axis of the post and the substrate normal.

concentration of the phthalic acid proved to be too low if this technique was used. A 20 microliter drop of a 10^{-3} molar solution of the dopant compound dissolved in methanol was then deposited on the surface and the alcohol allowed to dry. The sample was then ready for testing. The lifetime of this type of sample is approximately one day.

A post sample of this type is very durable and should last many months. It may be stripped of its silver and a fresh coating applied in order to use the sample in other experiments.

Apparatus

The experimental apparatus basically consisted of two continuous wave, inert gas lasers, a double Raman spectrometer, and assorted optical devices. An ultraviolet-visible spectrophotometer was used to take absorbance data on the SERS samples. A diagram of the experimental setup is shown in figure 2.3. Two continuous wave lasers were used as monochromatic sources of light. One was a Coherent Innova 90-K Krypton Ion laser (2.9), and the other was a Spectra-Physics Model 166 Argon Ion laser equipped with a model 265 power supply (2.10). Both lasers allow the user to choose between several characteristic laser wavelengths in order to span the optical region between the wavelengths 457.9 nm and 676.4 nm. Interference bandpass filters with a bandwidth of 3 nm were used with each wavelength in order to suppress extraneous plasma lines mixed with the laser line that might be scattered into the collection optics and be mistaken for Raman lines.

A Spectra-Physics Model 310-21 Polarization Rotator (2.11) was used in the beamline to adjust the polarization of the incident laser light.

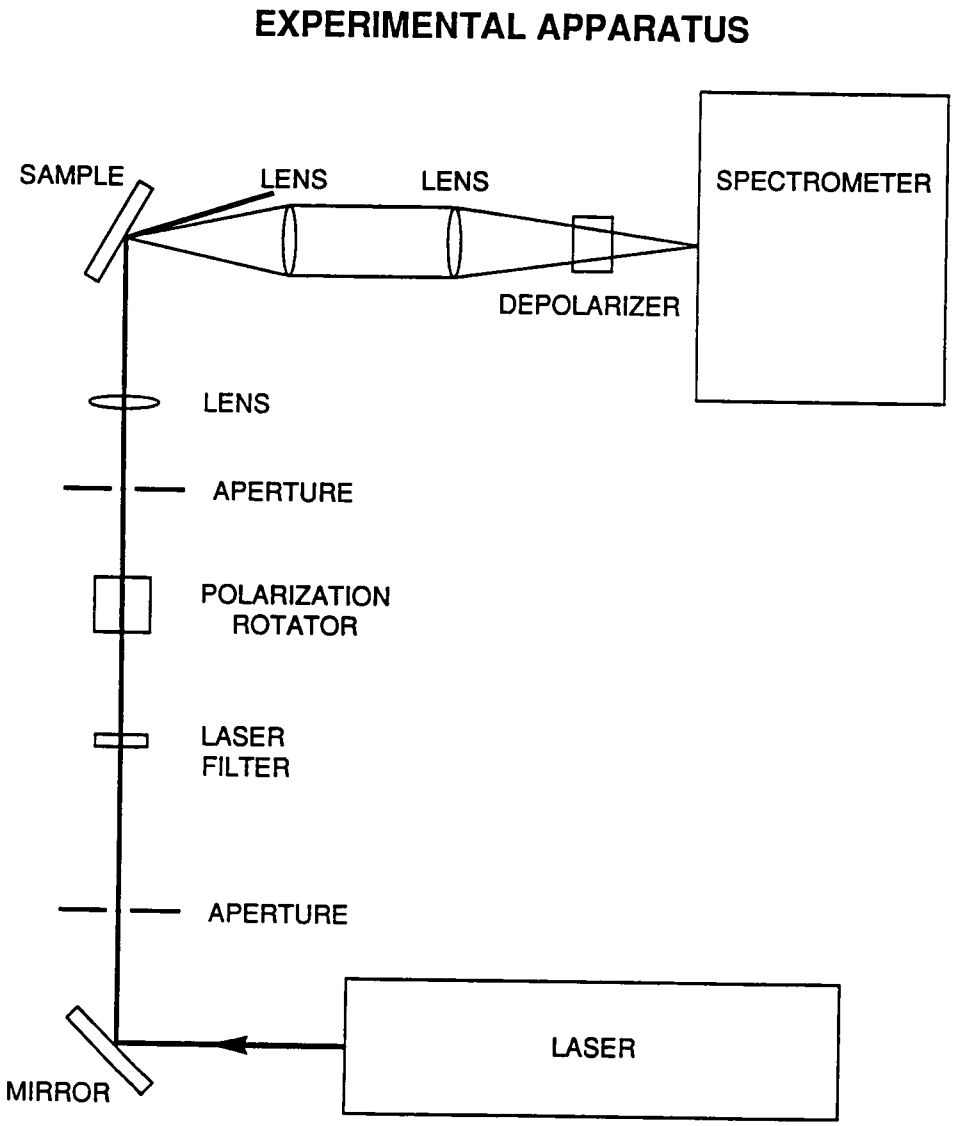

Figure 2.3. The experimental apparatus. Scattered light from the sample is collected near the specular beam.

The polarization rotator utilizes a Fresnel Rhomb (2.12) to allow the polarization vector to be rotated over 360 degrees throughout a wavelength region from 400 nm to 700 nm. The polarization rotator was used to orient the beam for either s polarization or p polarization with respect to the sample plane of incidence. No polarizing device was used in the beamline since each laser utilizes brewster angle windows on the front and rear of each tube that highly polarize the light.

Wavelength selection in both lasers is performed by tilting the rear prism assembly with respect to the longitudinal axis of the laser. Unfortunately, changing wavelengths also slightly alters the path of the beam so that some realignment was necessary after each wavelength change. This was performed by placing two apertures in the beamline after an adjustable mirror and then redirecting the beam through the apertures. The apertures were approximately two feet apart.

The entire set of collection optics including the sample holder was mounted on a standard optical bench and placed directly in front of the entrance slit of the spectrometer. The sample mount was attached to a rotation-translation stage. A lens was positioned to the side of the optical bench in order to focus the laser light onto the sample. The laser beam angle of incidence with respect to the sample normal and the scattering take-off angle with respect to the spectrometer entrance slit was chosen by adjusting the position of the final mirror and the sample orientation. The sample was always positioned so that the laser light was incident on the silvered side of the posts. Refer to figure 2.4. The particle spacing is very small relative to the wavelength of the incident light; therefore, even these incoherent sources combine to emit

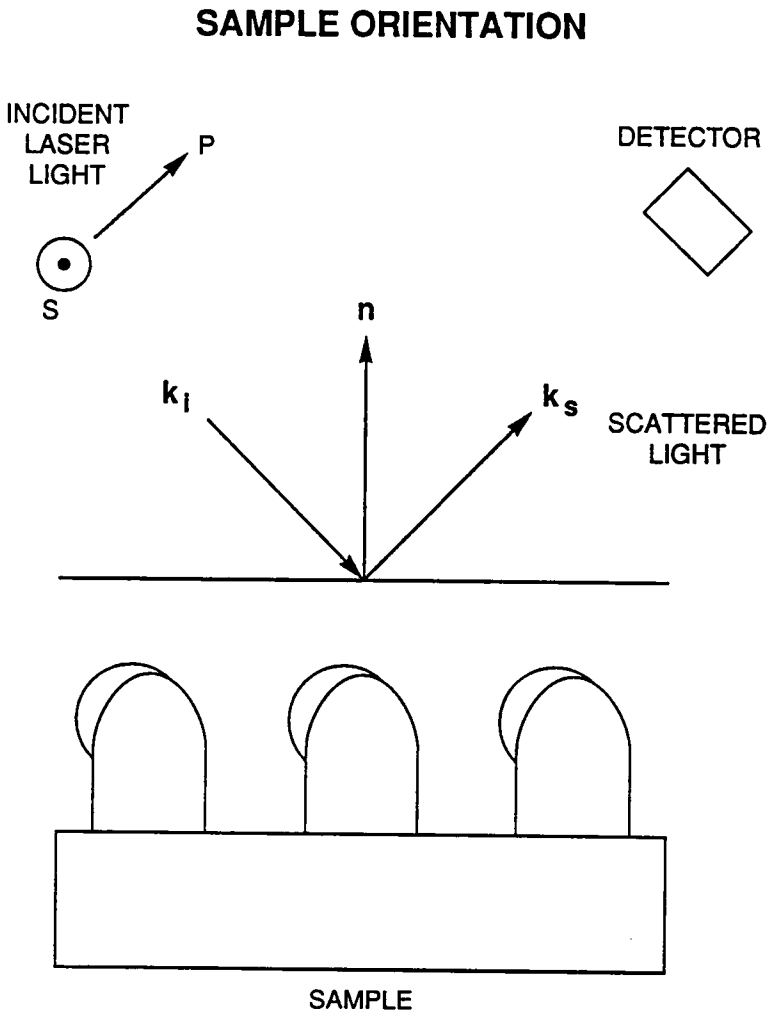

Figure 2.4. The sample orientation during the measurements. The laser light incident angle was 45 degrees with respect to the major post axis and the substrate normal. The spectrometer was positioned to collect light near the specular direction at 45 degrees.

coherently. As a result, most of the scattered Raman light is found close to the direction of the specular reflection. Therefore, data was taken close to the specular direction. A long focal length lens was used to focus the laser light onto the sample in order to confine the scattered light to a small solid angle.

A collection lens was placed in front of the sample at a distance equal to its focal length in order to collimate the scattered light. Another lens was used to refocus the light onto the spectrometer entrance slit. The wavelength response of the spectrometer was strongly polarization dependent. Consequently, a wedge depolarizer (2.13) was employed to effectively utilize the spectrometer sensitivity over the full optical region of the spectrum. The depolarizer is a birefringent crystal (quartz) (2.14) cut into a wedge and placed inside a cylindrical mount. As light passes through the wedge, one component of the polarization is retarded while the other is not. Since the thickness of the crystal varies across the surface, any beam of light that passes through the wedge will be depolarized. It is necessary, however, to use the entire surface of the wedge in order to effectively depolarize the light. Use of the depolarizer also allowed a spectrometer calibration for unpolarized light to be used in the data correction. The spectrometer response will be discussed later in this section.

Several attempts were made to reduce laser induced sample degradation due to high power densities by using unfocused laser light. Power densities of more than 3.8 watts/cm^2 degraded the surface and significantly reduced signal strengths by as much as 30 percent during seven minutes of continuous exposure. However, variations in

cross-sectional laser beam intensity due to the effects of laser cavity modes (2.15) required that the beam be focused to simulate a point scatterer. Focusing prevented variations in the beam intensity distribution on the sample from altering the distribution of light on the spectrometer gratings as laser lines were changed. A laser spot of approximately 1 mm in diameter and a low incident power of no more than 20 milliwatts proved to be the better method for achieving both goals. Incident power levels were measured with a laser light meter (2.16) positioned in front of the sample. The power was held constant for each laser line.

The spectrometer used in the experiments is a SPEX model J2615K00 double-Raman spectrometer equipped with two concave holographic gratings and a computer used to control the system (2.17). The gratings are appropriate for use in the region from 425 nm to 850 nm. The detector is a 2 inch diameter, 11 stage, Quanticon type, GaAs photomultiplier tube (2.18). It is housed inside a water-cooled, thermoelectric refrigeration chamber (2.19). The computer serves as a spectrometer controller and a data processor with 4 kilobytes of data storage. A schematic of the spectrometer is shown in figure 2.5. Data may be stored in memory and graphically displayed for analysis. A graph plotter is also interfaced with the computer. The entrance, intermediate, and final slits may be adjusted with verniers from zero to three millimeters in increments of one micron. The entrance shutter is equipped with several apertures of different heights to select portions of the entrance slit. Data was usually taken with the entrance and exit slits set at 0.5 mm and the intermediate slits set at 1 mm.

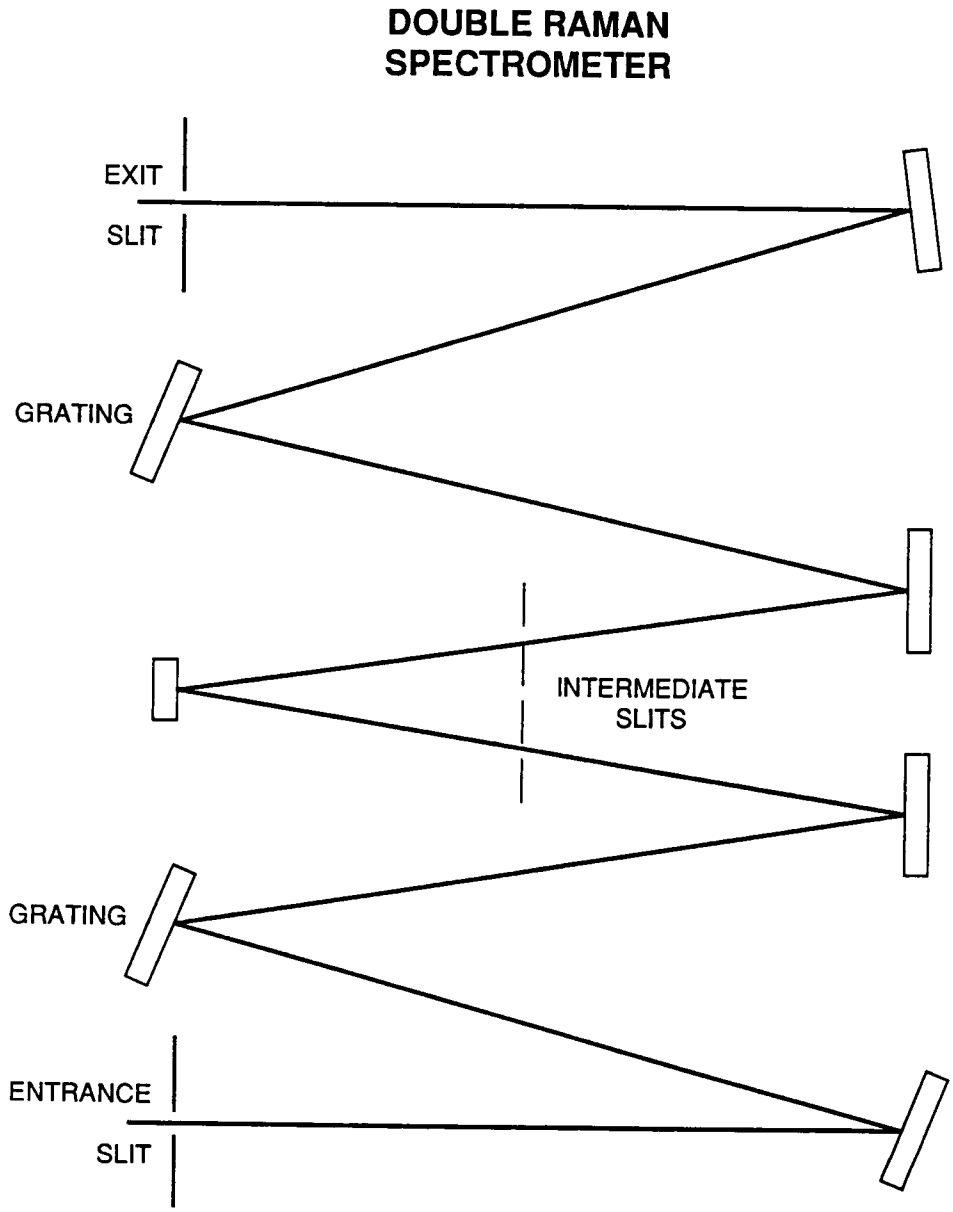

Figure 2.5. Schematic of the double Raman spectrometer. It contains two holographic gratings for high resolution.

The optical alignment was performed by positioning the lasers, the spectrometer entrance slit, and the center of the first interior spectrometer mirror in the same horizontal plane. This insured that the optics would collect the center portion of the scattered light cone. All other optical devices were positioned to retain the beam alignment.

A calibration of the spectrometer was performed in order to account for its wavelength and polarization dependence. The response is due primarily to the reflectance properties of the gratings. The spectrum of an NBS tungsten filament lamp was measured with the spectrometer for comparison with the spectral information provided with the lamp. Data points were taken in 400 wavenumber increments over the region from 450 nm to 750 nm. Three measurements were made: one for unpolarized light, one for light polarized parallel to the direction of the rulings (s-polarized), and one for light polarized perpendicular to the rulings (p-polarized). The response function of the system was obtained by normalizing the spectrometer data curve to the NBS data curve. The procedure was as follows. The NBS curve was scaled to equal the spectrometer curve at one wavelength. The response at that wavelength was defined to be one. The response at other wavelengths was determined by fitting the spectrometer curve to the NBS curve. The response factors are the numbers that perform the fit. Response curves for s and p polarizations were obtained in the same way by using polaroids in the beam during the measurements. Figure 2.6 is a graph of the response as a function of wavelength for unpolarized, s-polarized, and p-polarized light. The response for p polarized light in the wavelength region below

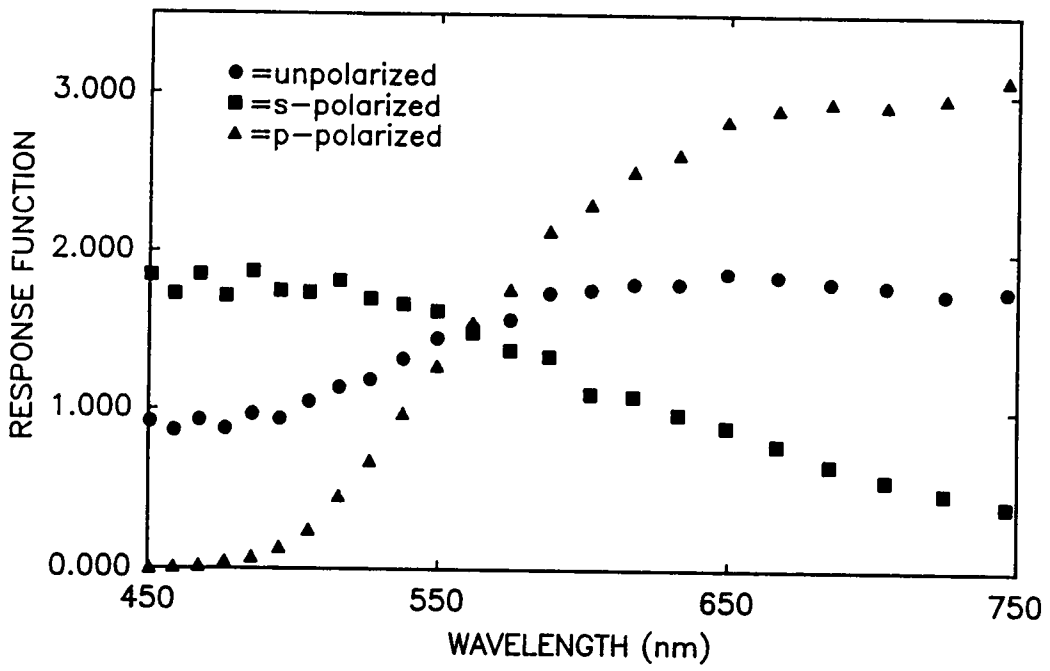

Figure 2.6. The spectrometer response curves. Circles represent unpolarized light, squares represent light polarized parallel to the grating rulings, and triangles represent light polarized perpendicular to the rulings.

500 nm was quite low. This was the justification for using the polarization scrambler when taking data.

Absorbance data was taken with a Shimadzu UV-250 recording spectrophotometer (2.20). The UV-250 has a double monochrometer equipped with one concave and one planar holographic grating. Figure 2.7 is a schematic of the system. The light sources are halogen and deuterium lamps. Absorbance and transmittance data may be taken between 190 nm and 900 nm. The sample chamber has adjustable mounts upon which the sample and a reference may be placed. In all cases the reference was a post sample with no silver. This was not an important factor, however, since a the optical properties of a bare post sample were no different than those of a quartz slide with no posts. The angle of incidence of the light with respect to the sample and reference may be chosen by rotating their respective holders. Polaroids placed in front of the sample and reference were used to polarize the incident light. A baseline correction for the polaroids was performed before a set of data was taken for a particular polarization.

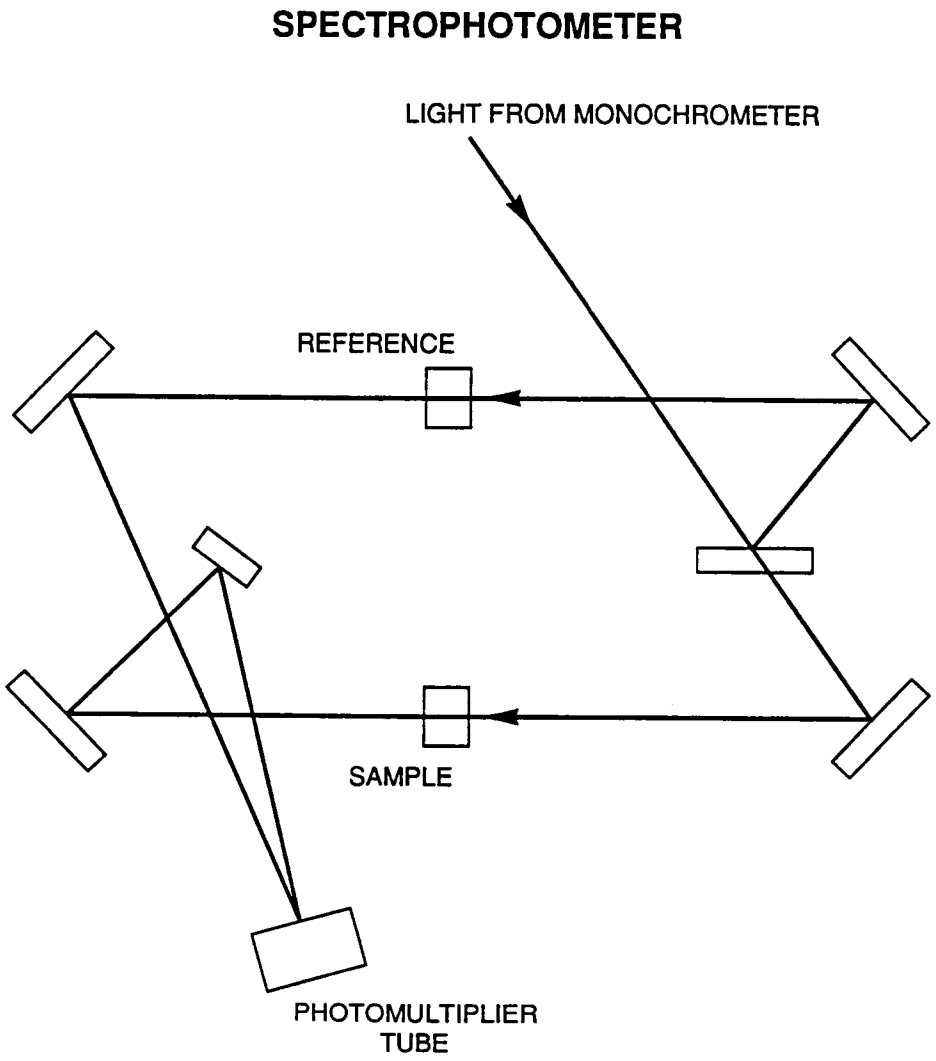

Figure 2.7. Schematic of the spectrophotometer. Light from the monochrometer passes through the sample and the reference.

CHAPTER III

EXPERIMENTAL RESULTS

Data

The objective in this experiment was to compare the intensity of the SERS signal of organic compounds on Raman active surfaces to their respective optical absorbance data. The substrates used for the analysis consisted of various sizes of submicron, silver coated, polystyrene spheres, metal island films of silver oblate spheroids, and silver coated silicon dioxide posts etched into the surfaces of microscope slides. The posts were either randomly arrayed with their major axes normal to the surface, or they were ordered and tilted.

The SERS signals from the sphere substrates were usually good; however, the substrates did not possess well defined optical properties. Reproducability of the signal was not as significant a problem with the sphere substrates as it was with the post substrates. The SERS signals for those sphere substrates that gave a signal were consistently between approximately 100 and 1500 counts per second. The SERS signals with all sphere sizes tended to increase steadily as the sphere density was increased to monolayer coverage. The evaporation thicknesses that tended to produce the best enhancements were about 30 percent of the sphere diameter. Refer to Moody in (3.1) for a more detailed analysis of SERS from sphere substrates.

Several attempts were made to measure SERS from the metal island films of silver discussed in chapter II; however, no successful measurements were made. Likewise, SERS signals from the tilted posts occasionally reached several hundred counts above background but were usually much less.

The random arrayed, silicon dioxide posts, however, gave measureable SERS signals and reasonable optical properties. In fact, the SERS signal in some cases reached 3000 to 4000 counts above the background with the same laser light intensity as was used on the other types of samples (less than 50 milliwatts). SERS intensities were usually several hundred counts above the background.

Varying the silicon dioxide etch rates during the sample fabrication process yielded posts of different heights. The maximum SERS intensity was usually obtained with a silver thickness of 100nm evaporated at 30 degrees incidence.

Although the SERS data discussed in this section was taken near the specular direction of the reflected beam, the SERS signals for many sample orientations with respect to laser beam incidence and scattering were tested for all of the substrates mentioned. The most intense signals were usually obtained for 60 degrees incidence with the detector aligned with the substrate normal.

While the SERS data varied somewhat from sample to sample, there was a general SERS profile that remained constant throughout the measurements. The samples discussed in this section are representative of the body of data. The section following this discussion contains an analysis of the data.

Two SERS samples consisting of randomly ordered posts where broken into pairs so that the Raman active compounds benzoic acid and phthalic acid could be analyzed simultaneously on a particular substrate. For both pairs of samples discussed here, the evaporation thickness was 30nm, and the evaporation angle of incidence was 25 degrees with respect to the surface normal. Since it was not practical to measure the entire Raman spectrum for each polarization and wavelength, only the 1006 cm-1 benzoic acid line and the 1051 cm-1 phthalic acid lines were measured. These lines are promenent in the spectra, and they produce good signals. Figures 3.1 and 3.2 contain graphs of the bulk Raman spectra of benzoic acid and phthalic acid, respectively.

Although contact with the surface does alter the electronic structure of the molecule slightly, the molecules do sufficiently retain their original electronic structures. This property can be seen by comparing the SERS spectra for benzoic acid in figure 3.3 and phthalic acid in figure 3.4 with their respective bulk Raman spectra.

The following text contains the plots of the relative Raman scattering intensities as functions of the incident wavelength and polarization for each sample. The relative intensity is the corrected magnitude of the peak height of the particular Raman line measured at each excitation wavelength. The corresponding optical data taken at the angle of laser incidence for each sample half is also presented. In all cases, the angle of laser light incidence was 45 degrees with respect to the sample normal, and the detector angle was 45 degrees with respect to the sample normal (i.e. the specular direction).

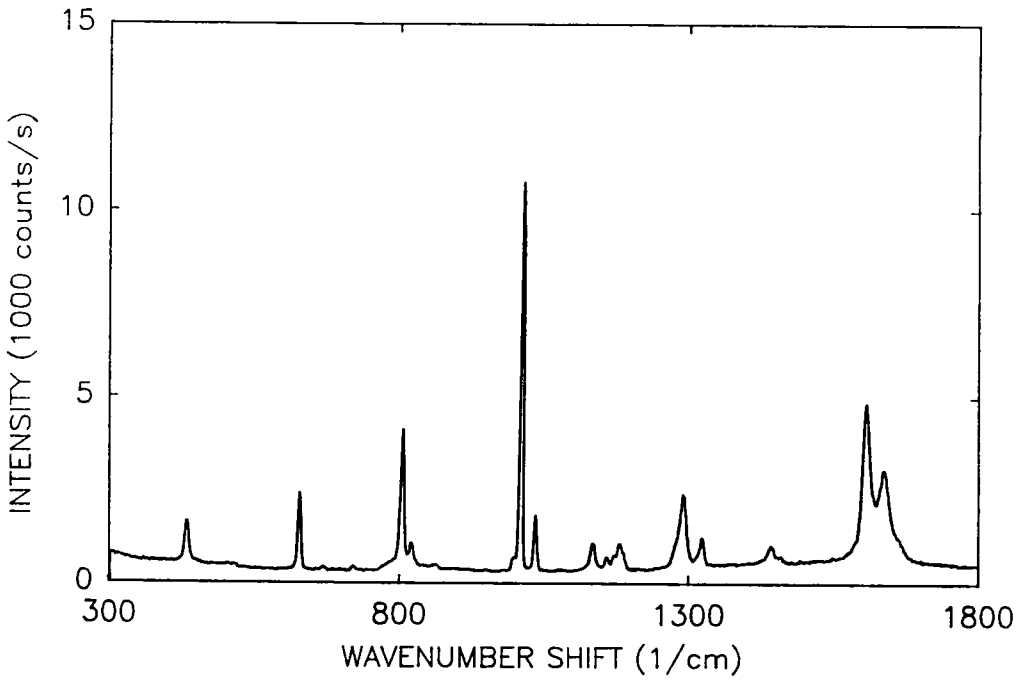

Figure 3.1. The bulk Raman spectra of benzoic acid.

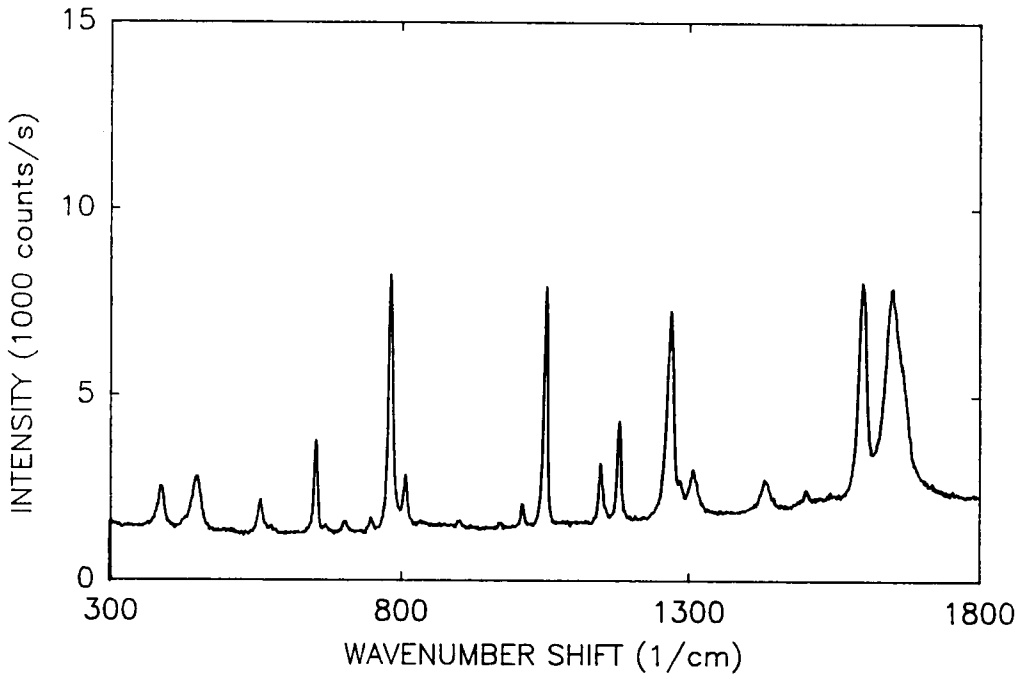

Figure 3.2. The bulk Raman spectra of phthalic acid.

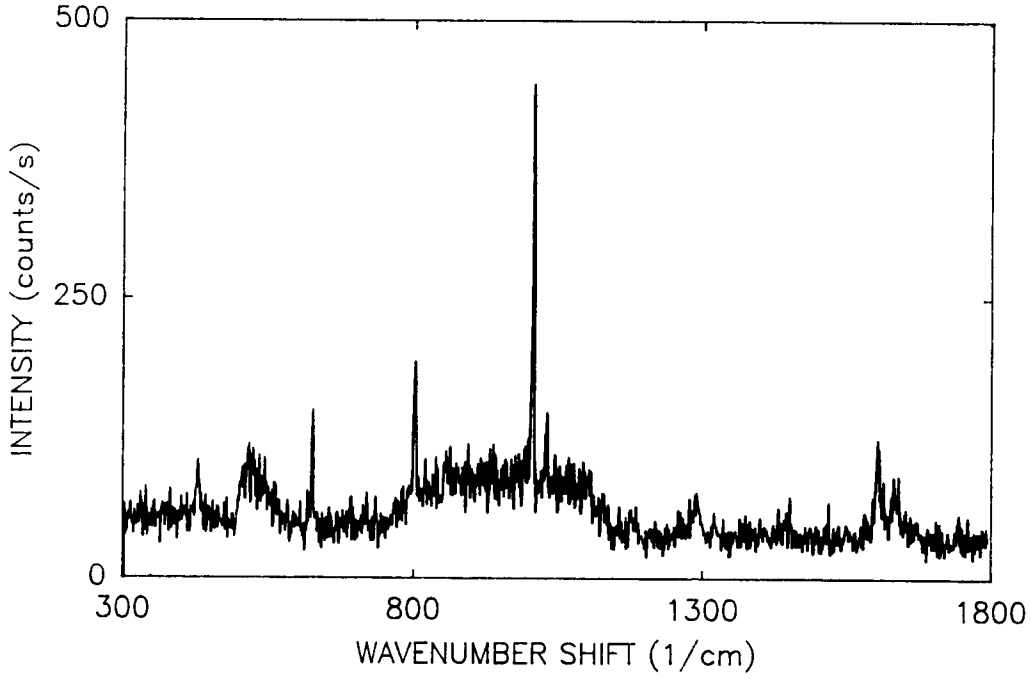

Figure 3.3. The surface-enhanced Raman spectra of benzoic acid.

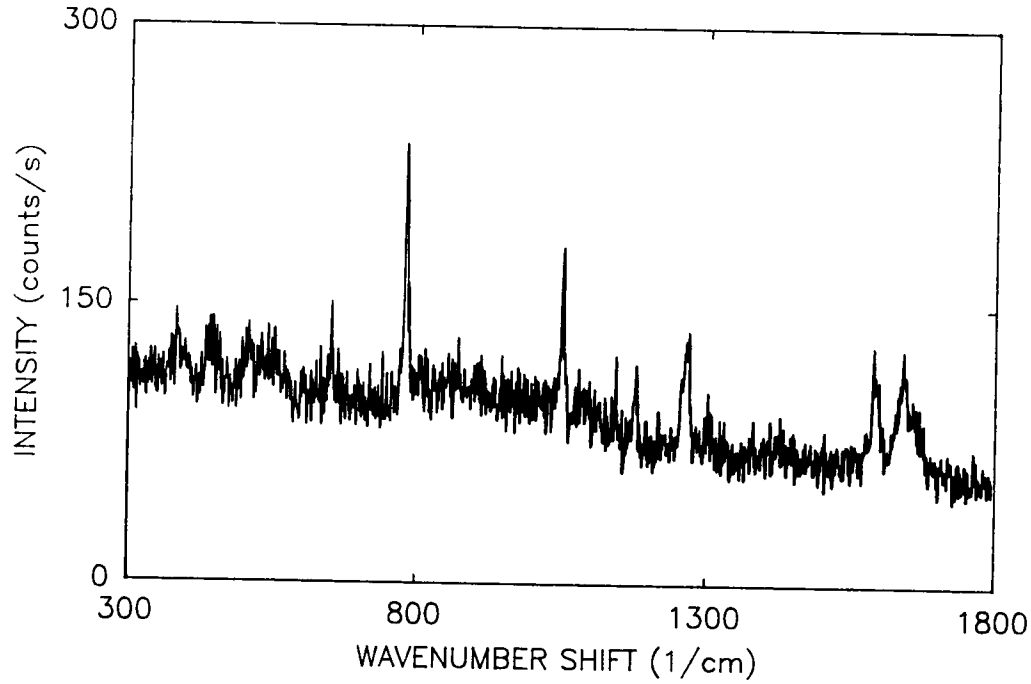

Figure 3.4. The surface-enhanced Raman spectra of phthalic acid.

Two corrections to the SERS data were performed in order to account for the spectrometer's wavelength and polarization sensitivity and the ω_o^4 dependence of the scattering cross section. A discussion of the spectrometer calibration and response corrections is in the apparatus section of the experimental chapter. The ω_o^4 dependence of the scattering cross section evident in eq. [1.52] is removed by dividing each SERS intensity by the appropriate ω_o^4 for the incident light.

In the following data discussion, sample 1 will refer to the post sample whose micrograph appears in figure 3.5. The post dimensions are approximately 220 nm tall and 60 nm in diameter. The micrograph of sample 2 appears in figure 3.6. The post dimensions are approximately 190 nm tall and 60 nm in diameter.

The relative intensity plot for a 1 x 10-3 molar solution of benzoic acid on sample 1 for s polarized incident light is contained in figure 3.7. The data shows a sharp rise from zero intensity in the blue region of the spectrum to a relative maximun at 501.7 nm. The relative intensity then tapers off gradually to zero in the red. The data for p polarized light in figure 3.8 shows a relative maximum at 514.5 nm which is about three fourths as great as for s polarized light. Several concentrations of phthalic acid were attempted on the other half of sample 1 under equivalent conditions with no success. The experimental error was determined by calculating the average intensity and standard deviation for ten random measurements on the sample. It was about fifteen percent for each line.

The optical data for s polarized light incident on sample 1 for both compounds is presented in figure 3.9. The benzoic acid data has a

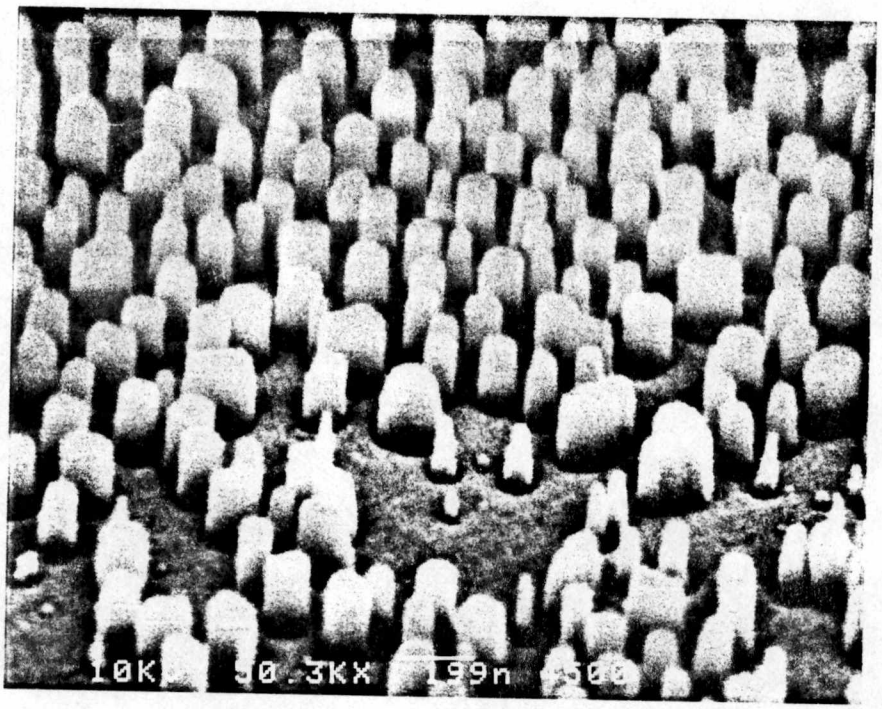

Figure 3.5. Electron micrograph of sample 1 at 50 degrees. This is a low density region in a scratch on the surface.

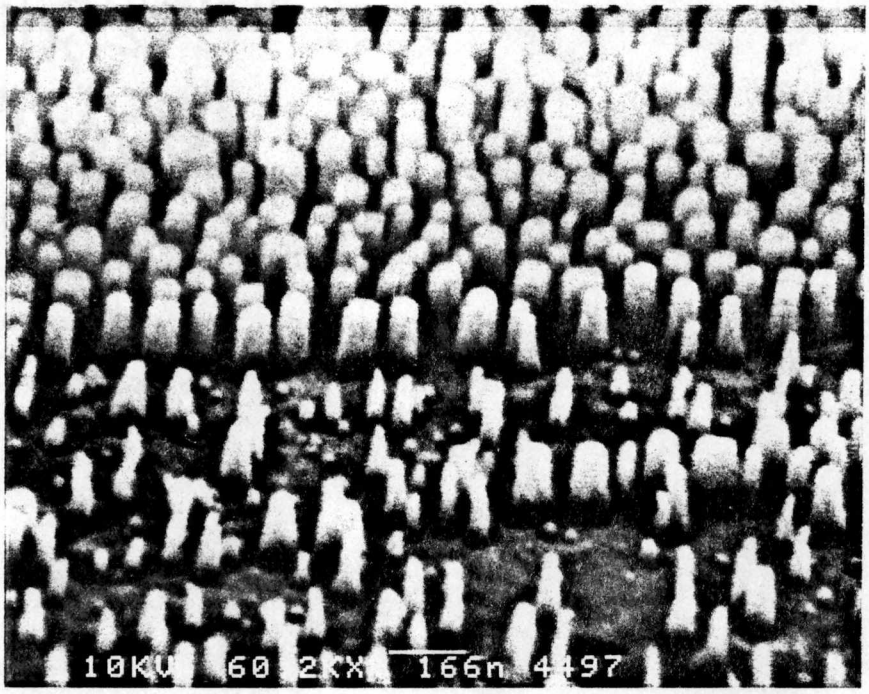

Figure 3.6. Electron micrograph of sample 2 at 50 degrees. This is a low density region in a scratch on the surface.

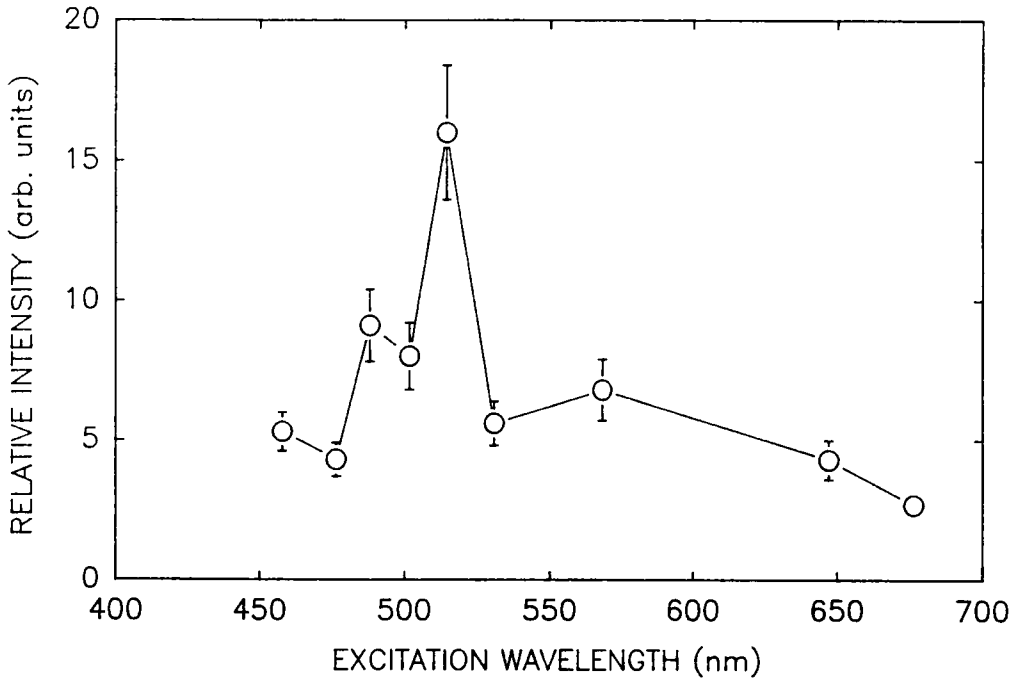

Figure 3.7. SERS relative intensity for s-polarized light incident on sample 1 coated with benzoic acid.

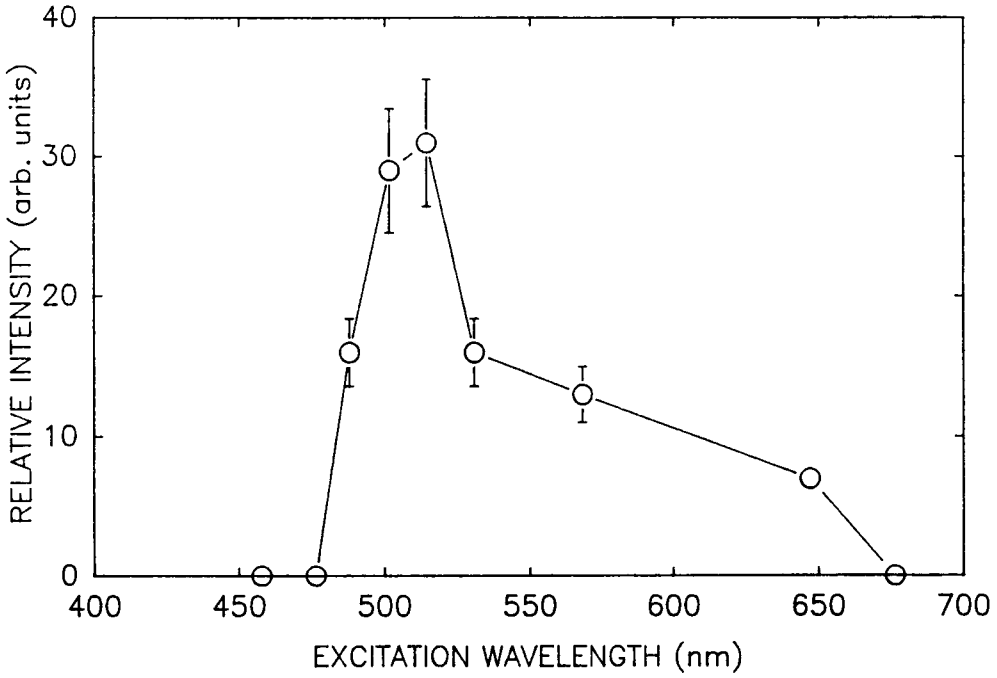

Figure 3.8. SERS relative intensity for p-polarized light incident on sample 1 coated with benzoic acid.

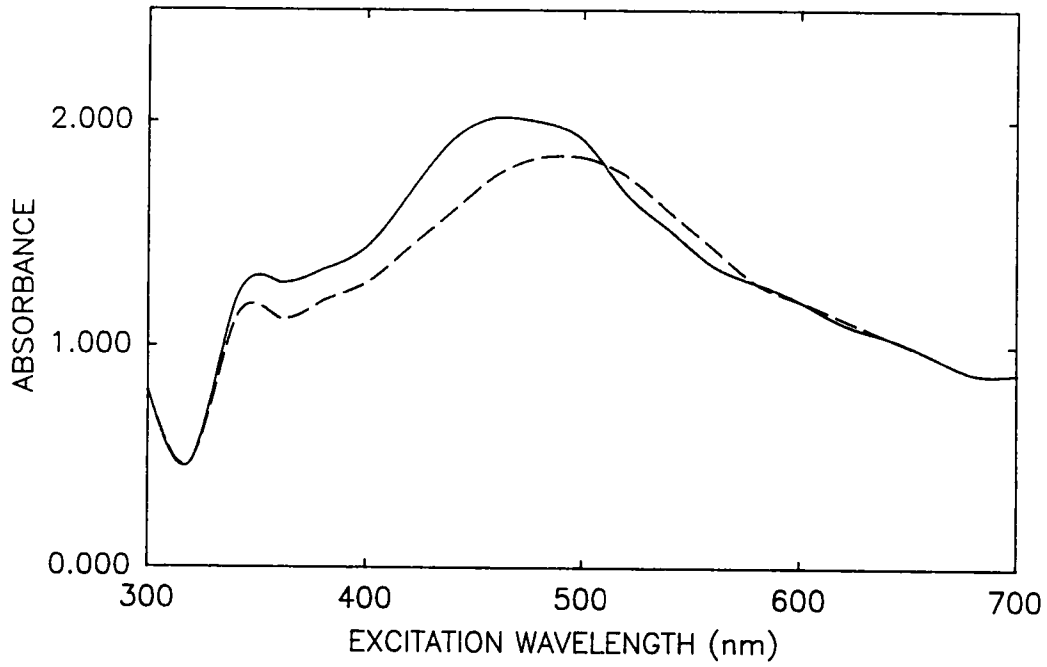

Figure 3.9. Optical absorbance data for s-polarized light incident on sample 1. The smooth curve represents benzoic acid coverage, and the dashed curve represents phthalic acid coverage.

maximum at 480 nn and the phthalic acid data at 500 nm. The p polarization optical data for both compounds on sample 1 is presented in figure 3.10. There is little difference in the absorbance curves with either compound. Both curves are featureless in the visible and show a flat absorbance of about one in that region. Both samples have a high energy resonance at approximately 360 nm for all polarizations and angles of incidence.

The SERS data for s polarized light incident on sample 2 doped with 1 x 10-3 molar benzoic acid is presented in figure 3.11. There is a strong maximum centered between 501.7 nm and 514.5 nm. The curve rises sharply from the blue and then gradually tapers off into the red. P polarization data in figure 3.12 shows a maximum centered at 514.5 nm which is slightly greater than that for s polarization. It also has the same general shape as its s polarization counterpart.

The SERS data for s polarized light incident on sample 2 with 1 x 10-3 molar phthalic acid is presented in figure 3.13. The data shows a broad curve that gradually rises from the blue to form a maximum centered at 647.1 nm. The curve then declines further into the red. P polarization data in figure 3.14 has the same general trend with a broad maximum centered at 647.1 nm. The experimental error was calculated for sample 2 in the same fashion as for sample 1.

Optical data on sample 2 for s polarized incident light with both compounds is in figure 3.15. The absorbance curve for benzoic acid on sample 2 peaks at 420 nm, whereas the curve for phthalic acid peaks at 440 nm. Both curves are quite broad, and they have the same shape. The benzoic acid substrate has a slightly higher absorbance at maximum than

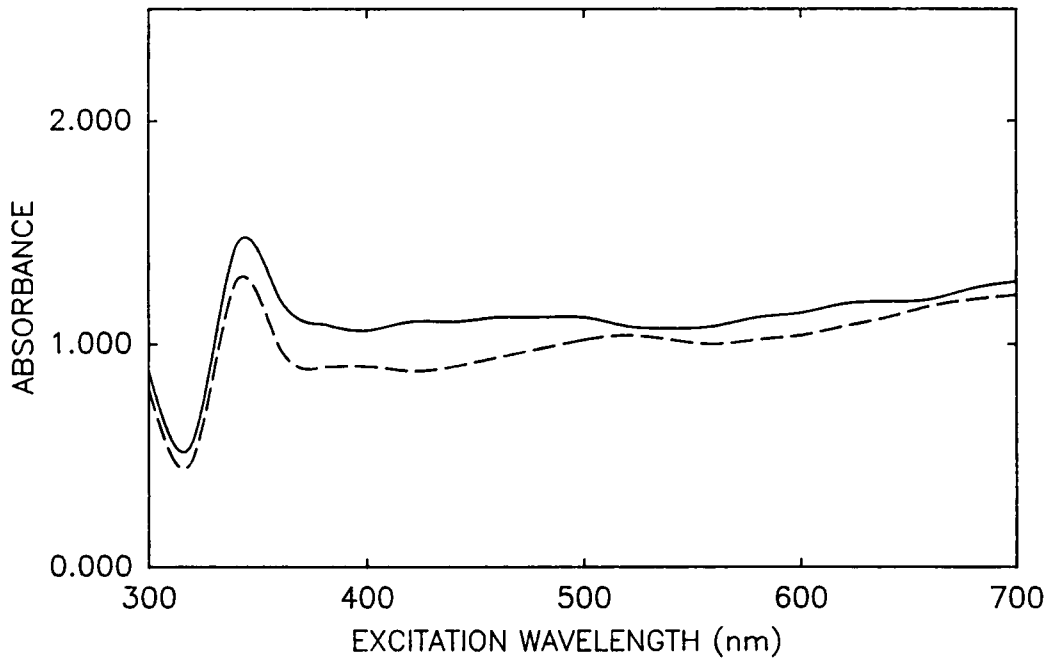

Figure 3.10. Optical absorbance data for p-polarized light incident on sample 1. The smooth curve represents benzoic acid coverage, and the dashed curve represents phthalic acid coverage.

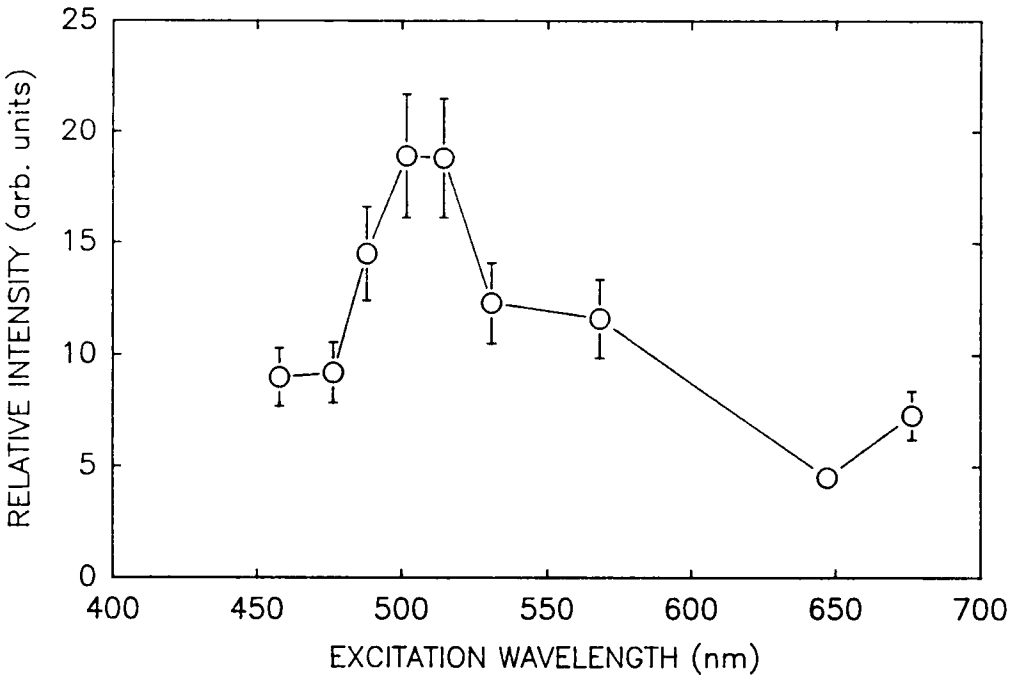

Figure 3.11. SERS relative intensity for s-polarized light incident on sample 2 coated with benzoic acid.

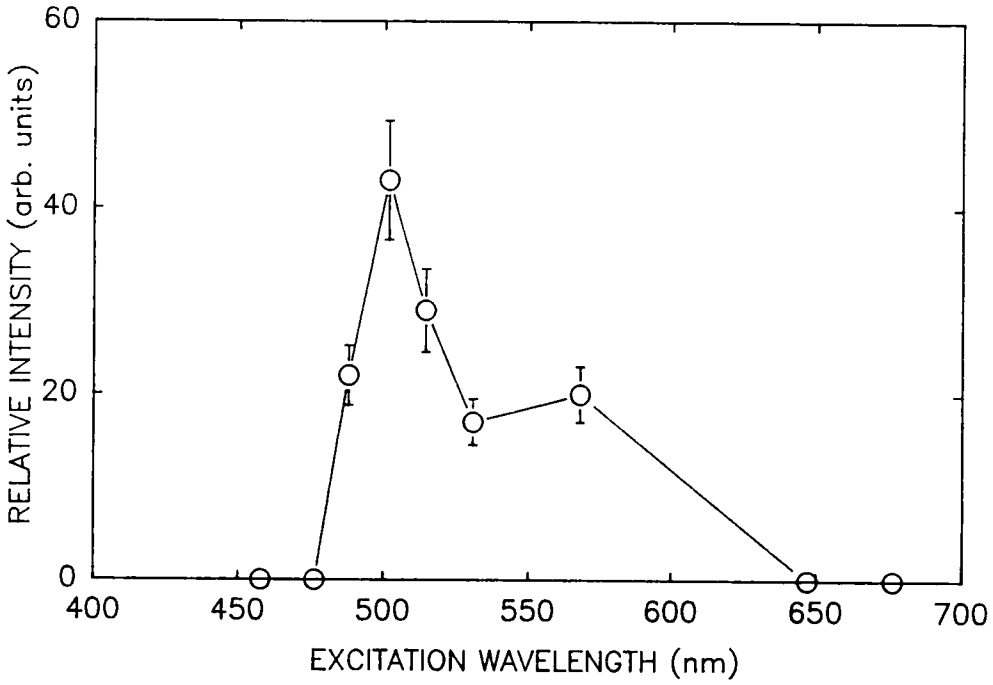

Figure 3.12. SERS relative intensity for p-polarized light incident on sample 2 coated with benzoic acid.

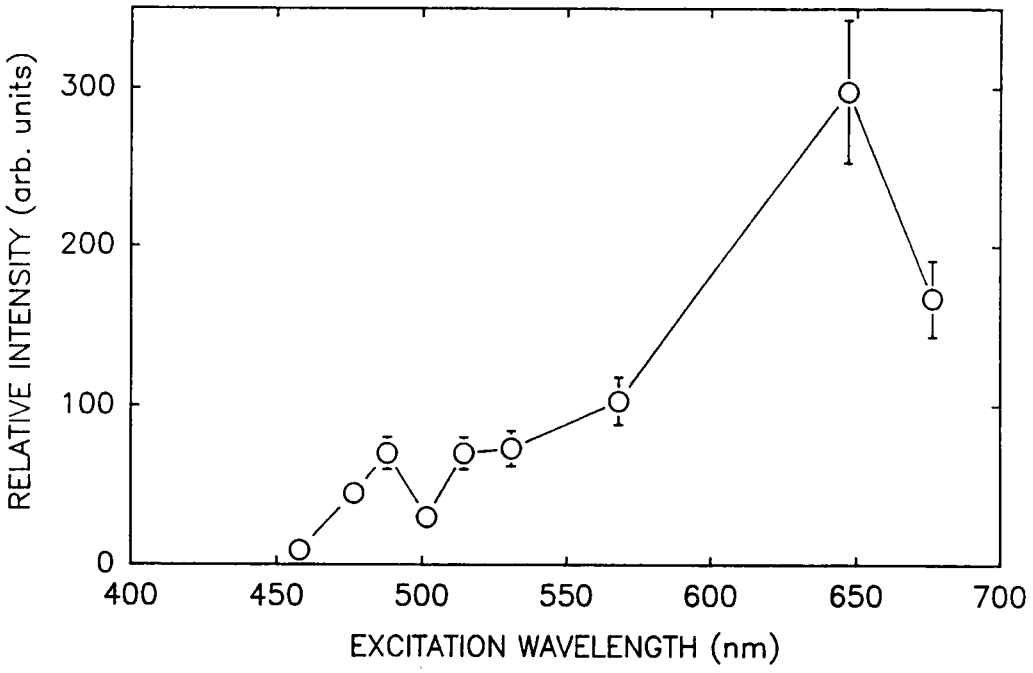

Figure 3.13. SERS relative intensity for s-polarized light incident on sample 2 coated with phthalic acid.

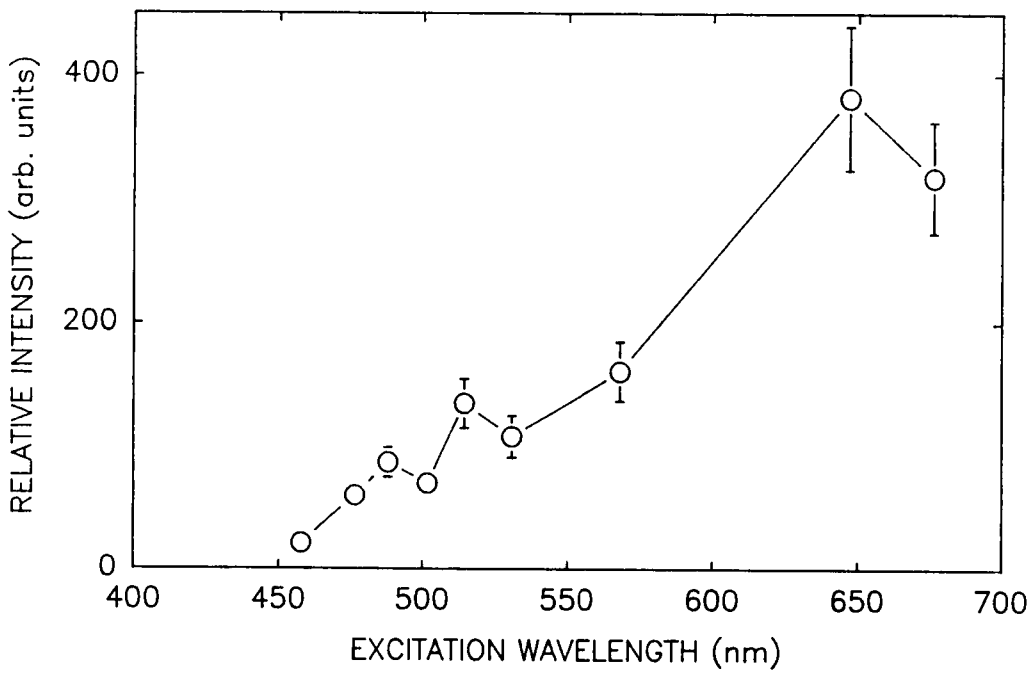

Figure 3.14. SERS relative intensity for p-polarized light incident on sample 2 coated with phthalic acid.

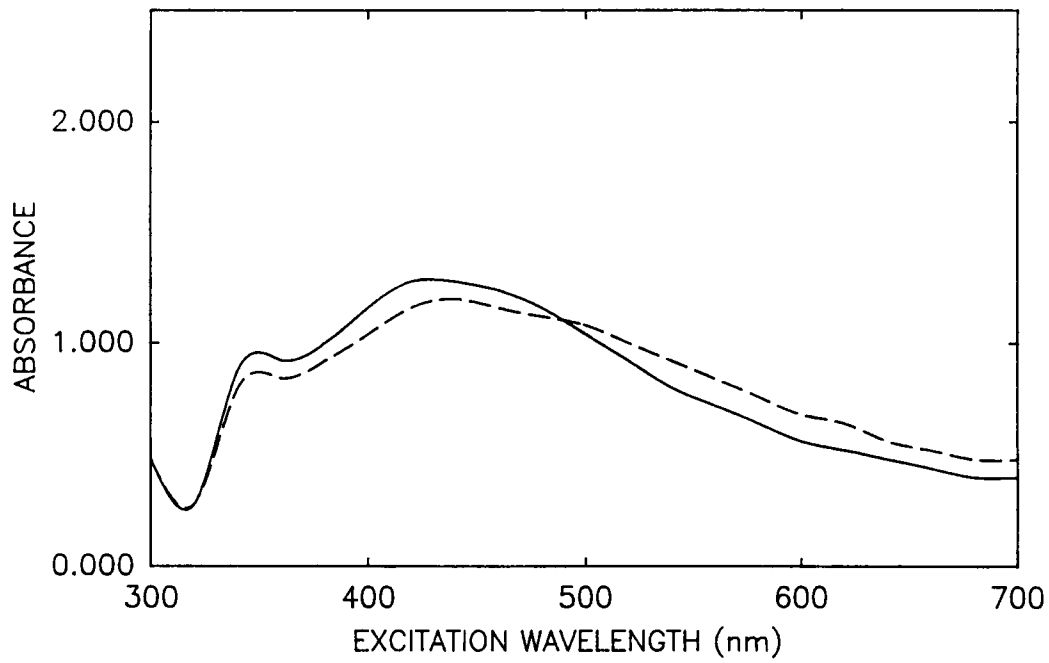

Figure 3.15. Optical absorbance data for s-polarized light incident on sample 2. The smooth curve represents benzoic acid coverage, and the dashed curve represents phthalic acid coverage.

the phthalic acid substrate. Optical data for p polarized incident light for both compounds is in figure 3.16. The benzoic acid substrate shows a broad maximum at 600 nm, and the phthalic acid substrate shows a broad maximum at 650 nm. Again, both samples have a high energy resonance at 360 nm.

Data Analysis

The SERS experiments performed in solution cells with electrochemically plated substrates show that the SERS enhancement follows the surface plasmon resonances of the particles (3.2). The same relationship was investigated for the dry substrates used in these experiments. The following discussion will demonstrate that there is a chemical effect involved in the enhancement as well as the overall electromagnetic effect.

The theoretical data presented in chapter I demonstrates that it is possible to model the substrate as a collection of particle shapes and sizes. Consider the p polarization, optical data for sample 2. The surface plasmon resonances of the benzoic acid and phthlalic acid substrates are both approximately 2.1 eV. This yields a minor to major axis ratio of 0.39. The particle is assumed to lie along the major axis of the silicon dioxide post. If the particle width is assumed to be the evaporation thickness with an angular correction, then the particle length is 33 nm. This is certainly a plausible particle size. This method of determining the particle size from the optical data could likewise be applied to sample 1.

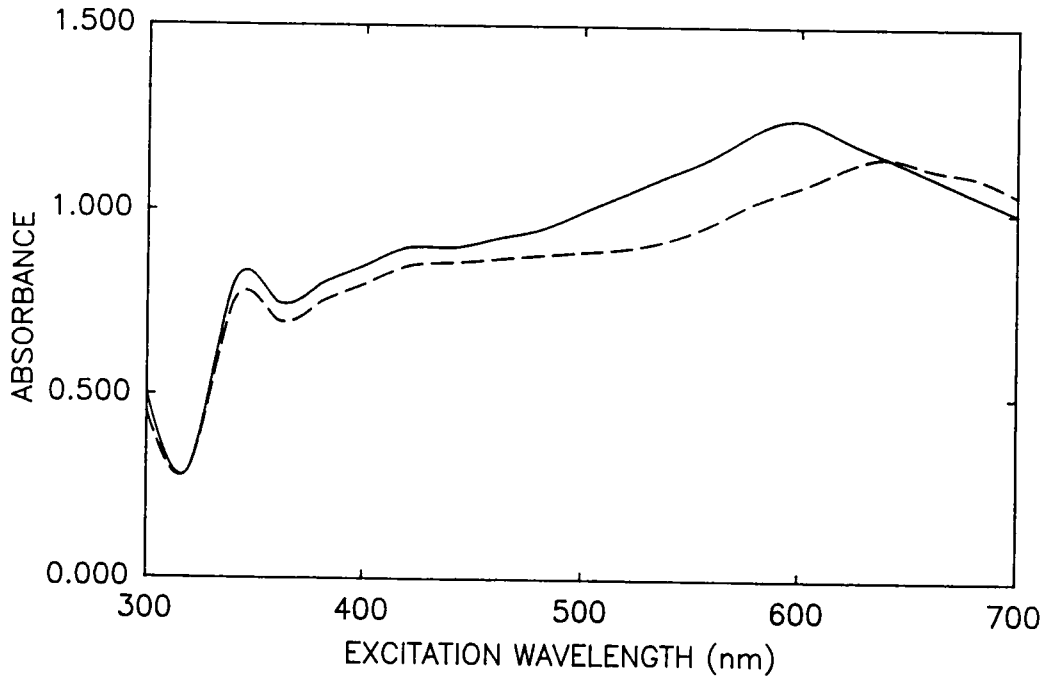

Figure 3.16. Optical absorbance data for p-polarized light incident on sample 2. The smooth curve represents benzoic acid coverage, and the dashed curve represents phthalic acid coverage.

The next step is to reconcile the optical data with the SERS data. This cannot be easily achieved, however. The p polarization optical data for sample 2 in figure 3.16 indicates that the SERS enhancement should have a maximum at 600 nm for benzoic acid and 650 nm for phthalic acid. The corresponding p polarization SERS data in figure 3.12 for benzoic acid shows that the maximum is blue shifted from the absorbance maximum by about 90 nm. The SERS data in figure 3.14 on sample 2 with phthalic acid shows an enhancement that reaches a maximum at the same wavelength as the absorbance maximum. For s polarized incident light on sample 2, the benzoic acid, SERS maximum in figure 3.11 is red shifted from the absorbance maximum in figure 3.15 by approximately 90 nm. The phthalic acid SERS maximum in figure 3.13 is red shifted by approximately 200 nm. Clearly, the position of the SERS enhancement maximum is not a sensitive function of the positions of the surface plasmon resonances of the substrate.

An analysis of the sample 1 data reveals that the SERS maxima for benzoic acid in figures 3.7 and 3.8 are at approximately the same wavelengths as in sample 2. Phthalic acid did not give an SERS signal from sample 1. Moreover, the optical properties shown in figures 3.9 and 3.10 are vastly different from sample 2. Sample 1 does not have a p polarization resonance in the visible. Clearly, there does not seem to be an obvious connection between the absorbance data and the SERS data. The plasmon resonances of both samples are also far too broad to account for the sharp structure of the SERS data. There is some chemical property or properties of the particular compound that determine the

positions, widths, and relative intensities of the SERS maxima. These properties obviously vary from one compound to another.

CONCLUSION

The purpose of this experiment was to analysis the role that the surface plasmon resonances of silver ellipsoids have on Surface-enhanced Raman scattering from dry, adsorbed molecules. The silicon dioxide, prolate post substrates used for the analysis gave measurable SERS signals in the wavelength region of interest for the two compounds used. These data were representative of the body of data derived from the several substrates tested during the course of the research. The original hypothesis that there should be coincidence between the wavelength and polarization dependences of the SERS enhancement and surface plasmon resonances was not shown to provide an explanation for the data. The positions of the maxima in the SERS data did not correspond to the positions of the surface plasmon resonances. Moreover, the peak-widths of the SERS data were far too sharp to be accounted for by the broad surface plasmon resonances of the samples.

The wavelength dependence of the SERS signal for a particular compound varied only slightly with a substrate change; whereas, the optical absorbance properties varied significantly. While the surface plasmon is certainly the fundamental cause of SERS, a significant, unspecified chemical dependence on the enhancement is the most logical explanation for the data.

It is not clear how the SERS of other compounds will behave on these and other surfaces. Since this data was taken for one Raman line of each chemical, the substrate interaction and wavelength dependence of

the many rotational and vibrational modes of each molecule is not known. If the wavelength and substrate dependences can be categorized for different compounds, then a new chemical classification system may be established.

Advances in instrumentation are also necessary in order to increase detection sensitivity. Together with advances in the fabrication of more easily characterized, highly effective SERS substrates, the puzzle may be solved. Certainly, more work needs to be done in these areas before an explanation is available.

LIST OF REFERENCES

REFERENCES

[I.1] M. Fleischmann, P. J. Hendra, and A. J. McQuillan, Chem. Phys. Lett. 26, p. 163 (1974).

[I.2] D. L. Jeanmaire and R. P. Van Duyne, Jour. Electroanal. Chem., 84, p. 1 (1977).

[I.3] J. A. Creighton, M. G. Albrecht, R. E. Hester, and J. A. D. Matthew, Chem. Phys. Lett. 65, p. 65 (1978).

[I.4] P. F. Liao in Surface-enhanced Raman Scattering, R. K. Chang and T. E. Furtak, eds. (Plenum, New York, 1982).

[1.1] B. H. Bransden and C. J. Joachain, Physics of Atoms and Molecules, (Longman Group Ltd., New York, 1983), p. 436.

[1.2] A. Campion in Vibrational Spectroscopy of Molecules on Surfaces, J. T. Yates, Jr. and T. E. Madey, eds. (Plenum, New York, 1987), p. 348.

[1.3] Ibid, p. 355.

[1.4] P. F. Liao and Woukan, Jour. Chem. Phys., 76, p.751. (1982).

[1.5] M. R. Philpott, Jour. Chem. Phys., 62, p. 1812 (1980).

[1.6] H. Metiu in Chang and Furtak, Op. cit., p. 2.

[1.7] P. A. M. Dirac, Quantum Mechanics, (Oxford Univer. Press,1978), p. 248.

[1.8] J. D. Jackson, Classical Electrodynamics, (Wiley and Sons, New York, 1975), p. 412.

[1.9] Ibid, p. 272.

[1.10] Ibid, p. 412.

[1.11] M. C. Buncick, Ph.D. dissertation, (Univer. of Tenn., Knoxville, 1987), p. 18.

[1.12] B. Illman and T. L. Ferrell, private communication.

[2.1] J. W. Little and M. C. Buncick, private communication.

[2.2] R. Moody, Masters thesis, (Univer. of Tenn., Knoxville, 1986), p. 46.

[2.3] M. C. Buncick, private communication.

[2.4] Esco Products, Inc., 171 Oak Ridge Rd., Oak Ridge NJ 04738.

[2.5] Cole-Palmer Instr. Co., 7425 N. Oak Ridge Ave., Chicago IL 60648.

[2.6] Air Products and Chemicals, Inc., Box 2802, Allentown PA 18105.

[2.7] R. D. Mathis Co., 2840 Grundy Ave., Long Beach CA 90806.

[2.8] Buncick, Op. cit., p. 73.

[2.9] Coherent Laser Products Div., 3210 Porter Dr., Palo Alto CA 94303.

[2.10] Spectra-Physics Laser Instr. Div., 1250 W. Middlefield Rd., Mt. View CA 94042.

[2.11] Ibid.

[2.12] E. Hecht and A. Zajec, Optics, (Addison-Wesley, MA, 1979), p. 250.

[2.13] Oriel Corp., 250 Long Beach Blvd., PO Box 877, Stratford CT 06497.

[2.14] Hecht and Zajec, Op. cit., p. 235.

[2.15] Ibid, p. 483.

[2.16] Scientech Inc., 5649 Arapahoe Ave., Boulder CL 80303.

[2.17] SPEX Industries Inc., PO Box 798, Metuchen NJ 08840.

[2.18] RCA Electro-optics and Devices, Lancaster PA 17604.

[2.19] Products for Research Inc., 88 Holten St., Danvers MA 01923.

[2.20] Shimadzu Scientific Instr. Inc., 7102 Riverwood Dr., Columbia MD 21046.

[3.1] Moody, Op. cit., p. 23.

[3.2] J. A. Creighton, C. G. Blatchford, and M. G. Albrecht, Jour. Chem. Soc., Faraday Trans. 2, 75, p. 790.

VITA

David Lewis Bailey was born on September 3, 1961 in Moultrie, Ga. He is the son of Arthur C. Bailey, Jr. and Velma Carol Bailey. David graduated from West High School in Knoxville, Tennessee in June of 1979. The following September, he entered the University of Tennessee, Knoxville. He was awarded a Bachelor of Arts degree with a major in Physics in June of 1983. In January of 1984, he enrolled as a graduate student at the University of Tennessee and was employed as a graduate research assistant at Oak Ridge National Laboratory. He was awarded the Master of Science degree with a major in Physics in August of 1988.